

Broadened-beam Uniform Rectangular Array Coefficient Design in LEO SatComs Under Quality of Service and Constant Modulus Constraints

Weiting Lin, *Student Member, IEEE*, Yuchieh Wu, Borching Su, *Member, IEEE*

Abstract—Satellite communications (SatComs) are anticipated to provide global Internet access. Low Earth orbit (LEO) satellites (SATs) have the advantage of providing higher downlink capacity owing to their smaller link budget compared with medium Earth orbit (MEO) and geostationary Earth orbit (GEO) SATs. In this paper, beam-broadening algorithms for uniform rectangular arrays (URAs) in LEO SatComs were studied. The proposed method is the first of its kind that jointly considers the path loss variation from SAT to user terminal (UT) due to the Earth’s curvature to guarantee quality of service (QoS) inspired by the synthesis of isoflux radiation patterns in the literature, constant modulus constraint (CMC) favored for maximizing power amplifier (PA) efficiency, and out-of-beam radiation suppression to avoid interference. A URA design problem is formulated and decomposed into two uniform linear array (ULA) design subproblems utilizing the idea of Kronecker product beamforming to reduce the computational complexity of designing URA. The non-convex ULA subproblems are solved by a convex iterative algorithm. Simulation results reveal the advantages of the proposed method for suppressing out-of-beam radiation and achieving design criteria. In addition, channel capacity evaluation is carried out and shows that the proposed “broadened-beam” beamformers can offer capacities that are at least four times greater than “narrow-beam” beamformers employing an array steering vector when beam transition time is taken into account. The proposed method holds potential for LEO broadcasting applications such as digital video broadcasting (DVB).

Index Terms—Satellite communications (SatComs), low Earth orbit (LEO) satellite, beam pattern synthesis, beam-broadening algorithm, isoflux radiation pattern, constant modulus constraint (CMC), Kronecker product beamforming, uniform rectangular array (URA), uniform linear array (ULA), Digital video broadcasting (DVB).

I. INTRODUCTION

SATELLITE communications (SatComs) are anticipated to provide global Internet access and facilitate seamless connections worldwide [1]–[3]. Owing to the advancements in satellite (SAT) payload design and launching processes, the cost of deploying Low Earth orbit (LEO) SATs has become affordable for business service providers [4]. LEO SAT constellations, e.g., Starlink, OneWeb, Kuiper, and Lightspeed, have been deployed in recent years [4]. LEO SATs hold the potential for delivering high-speed broadband services with low latency due to their smaller link budget and shorter propagation delay compared with medium Earth orbit (MEO) and geostationary Earth orbit (GEO) SATs [1]. To achieve higher downlink capacity, beamforming is essential in overcoming the link budget. If the transmitted signal phase is adjusted according to the array steering vector for beamforming purposes, the main lobe beamwidth is inversely proportional to the

antenna aperture when the signal wavelength is fixed [5]. SATs equipped with larger array sizes can achieve greater array gain, resulting in higher downlink capacity. However, SAT beam coverage decreases as the antenna aperture increases, and more beams are required to cover the specific service areas. Although beam hopping technologies can be utilized for beam resources management [6]–[8], system complexity increases significantly as the increase of beam numbers or the demand for various services [7], [8]. Also, frequent beam switching increases beam transition time delays that stem from the data queuing time on SATs [6]–[8]. In light of this, it is crucial for SATs equipped with large antenna sizes to pursue high downlink capacity while simultaneously serving UTs over wide areas, especially for downlink broadened-beam transmission.

For broadened-beam applications in SatComs, isoflux radiation patterns have been considered to achieve uniform received power density within SATs service areas [9]–[13]. Isoflux radiation patterns with various beamwidths (16° [13], 18° [9], 42° [12], 90° [11] and 102.66° [10]) were proposed. In [9]–[13], fitness functions were constructed and minimized through evolutionary algorithms for approximating the pre-defined isoflux radiation pattern. In [9], a genetic algorithm was applied, and aperiodic planar arrays were designed. In [10], an evolutionary multi-objective optimization method was employed, and sparse concentric rings arrays were designed. In [11], a firefly algorithm was utilized, and non-uniformly spaced linear and planar arrays were implemented. In [12], genetic algorithm and particle swarm optimization methods were applied, and an ellipse dipole antenna array was designed. In [13], a differential evolution algorithm was presented, and ULA of a shared subarray architecture was designed. Nevertheless, [9]–[13] did not include constant modulus constraint (CMC) when synthesizing isoflux radiation patterns. In SAT applications, beamformer design with CMC is desired to enable power amplifiers (PAs) to operate at near compression points for maximizing efficiency [14]–[16]. PA efficiency is essential to reduce power consumption [14], especially on SAT where only limited power resources are available [17]. Also, high PA efficiency prevents wasted power that generates heat, potentially leading to circuitry overheating [15]. Thus, the algorithms that synthesize isoflux radiation patterns without considering CMC in [9]–[12] may not be practical for SAT applications. One possible reason for not considering CMC in [9]–[12] could be the difficulties of considering equality constraints in evolutionary algorithms [18]–[20].

Beam-broadening algorithms considering CMC or dynamic range ratio (DRR) constraints have been studied in [21]–[27]. In [21]–[23], semidefinite relaxation (SDR) techniques and low-rank minimization approaches were applied. However, the approaches did not ensure obtaining a rank-one solution, and thus the CMC may not be met. Recently, alternating direction method of multipliers (ADMM)-based methods have been applied in beam pattern synthesis [24]–[26]. In [24], the objective was to minimize the ratio of peak sidelobe level (PSL) to the main lobe lower bound considering CMC, and it is solved by an ADMM-based method with a bisection method. In [25], the objective was to minimize PSL with given main lobe variation under CMC and DRR constraint. An ADMM-based method with a second-order complex Taylor expression was taken on. In [26], the minimum array directivity in main lobe regions was maximized considering DRR constraint. In [27], the closed-form analytic expression of phase-only broadened beam pattern was derived. Although beam-broadening methods with CMC or DRR constraint were discussed in [21]–[27], none of them were specifically designed for LEO SAT applications. They did not consider the variation of path loss from SAT to UT due to the Earth’s curvature, and thus can not guarantee QoS (i.e., the received signal-to-noise ratio (SNR)) in SAT service areas.

In this paper, we study beam-broadening algorithms for uniform rectangular arrays (URAs) in LEO SatComs. The design criteria include considering the path loss variation between SAT and UT due to the Earth’s curvature to guarantee QoS inspired by the synthesis of isoflux radiation pattern in [9]–[13], achieving CMC for maximizing PA efficiency, and minimizing the power leakage in out-of-beam areas to prevent interference. The URA design problem is formulated and decomposed into ULA design subproblems with the idea of Kronecker product beamforming [28]–[31] to reduce the computational complexity of designing URA. The non-convex ULA design subproblems are solved by a convex iterative algorithm. Additionally, channel capacity analysis is conducted to compare the capacity of the proposed “broadened-beam” beamformers with that of “narrow-beam” beamformers utilizing an array steering vector when beam transition time is taken into account.

The remainder of the paper is organized as follows. In Section II, the system model is introduced and the baseband equivalent transceiver model is derived. In Section III, the received SNR is derived considering the link budget, and the optimization problem of broadened-beam URA coefficient design in LEO SatComs under QoS and constant modulus constraints is formulated. In Section IV, the method of decomposing the URA design problem into ULA design subproblems is introduced, and the proposed algorithm is presented. In Section V, numerical results reveal the advantages of the proposed algorithm to achieve the design criteria, and channel capacity evaluation of “narrow-beam” and “broadened-beam” beamformers are conducted. Finally, conclusions are made in Section VI and suggestions are provided for future research.

Notations: Boldface upper case letters represent matrices, boldface lower case letters represent column vectors, and italic letters represent scalar, e.g., \mathbf{x} , \mathbf{X} , and x . The m -

th entry of \mathbf{x} and (m, n) -th entry of \mathbf{X} are denoted by x_m and $[\mathbf{X}]_{m,n}$. The M -dimensional complex vector space and $M \times N$ -dimensional complex matrix space are expressed as \mathbb{C}^M and $\mathbb{C}^{M \times N}$. Operators $(\cdot)^*$, $(\cdot)^T$, and $(\cdot)^H$ denote complex conjugate, transpose, and conjugate transpose. The set of all real numbers is denoted by \mathbb{R} , and \mathbb{R}_+ denotes the set of all positive real numbers. Zero-based indexing is applied, and \mathbb{Z}_M stands for the set $\{0, 1, \dots, M-1\}$ for any positive integer M . \mathbb{H}_+^M denotes the set of all $M \times M$ positive semidefinite matrices. Operators $\mathbb{E}\{\cdot\}$, $|\cdot|$, and \otimes denote expectation, modulus of a complex scalar, and Kronecker product. Functions $\text{Tr}\{\mathbf{X}\}$, $\text{vec}(\mathbf{X})$ and $\text{rank}(\mathbf{X})$, are trace, column-wise vectorization and rank of matrix \mathbf{X} . The inner product of two vectors \mathbf{x} and \mathbf{y} is represented as $\langle \mathbf{x}, \mathbf{y} \rangle$.

II. SYSTEM MODEL

In this section, we introduce the uniform rectangular array (URA), SAT transmitter (Tx) hybrid beamforming system model, UT receiver (Rx) system model, and the baseband equivalent transceiver models.

A. Uniform Rectangular Array (URA)

Consider the URA consisting of $M_x \times M_y$ array elements in Fig. 1a. Antenna elements are placed at the grid of x - y plane with antenna element spacing d_e . The URA element position vector is defined as $\mathbf{r}(m, l) = [md_e, ld_e, 0]^T$, $m \in \mathbb{Z}_{M_x}$, $l \in \mathbb{Z}_{M_y}$. The URA look direction is defined as $\boldsymbol{\kappa}(\theta, \phi) = [\sin(\theta) \cos(\phi), \sin(\theta) \sin(\phi), \cos(\theta)]^T$, where $\theta \in [0, \frac{\pi}{2}]$ is the SAT elevation angle and $\phi \in [0, 2\pi]$ is the SAT azimuth angle. The propagation delay of the antenna element at position $\mathbf{r}(m, l)$ relative to the antenna element at position $\mathbf{r}(m=0, l=0)$ is

$$\tau_{m,l}(\theta, \phi) = \frac{\langle \mathbf{r}(m, l), \boldsymbol{\kappa}(\theta, \phi) \rangle}{c} = \frac{md_e \sin(\theta) \cos(\phi) + ld_e \sin(\theta) \sin(\phi)}{c}. \quad (1)$$

B. SAT Transmitter (Tx) and UT Receiver (Rx) System Model

SAT transmitter (Tx) hybrid beamformer system model is depicted in Fig. 1b. Assume that Tx beamformer possesses $N_x \times N_y$ RF chains, $M_x \times M_y$ antenna elements, and the subarray size is $Q_x \times Q_y$, where $Q_x = \frac{M_x}{N_x}$ and $Q_y = \frac{M_y}{N_y}$. For beamforming purposes, amplitude $a_{i,j}$, $\forall i \in \mathbb{Z}_{N_x}$, $j \in \mathbb{Z}_{N_y}$, and phase shifters with phase adjustment $\phi_{m,l}$, $\forall m \in \mathbb{Z}_{M_x}$, $l \in \mathbb{Z}_{M_y}$, are applied to the transmitted signal. Let $s[n]$ be a constant modulus signal to be transmitted which is multiplied with amplitude $a_{i,j}$, converted to the continuous-time domain through a discrete-time to continuous-time (D/C) converter with sampling period T_s , shaped with transmitting pulse $p_T(t)$, up-converted to carrier frequency f_c , enlarged by PA with gain factor β , passed through 1 to $Q_x Q_y$ power divider and phase shifters. Define the URA beamforming coefficient matrix \mathbf{W} as

$$[\mathbf{W}]_{m,l} = \sqrt{\frac{1}{Q_x Q_y}} a_{i,j} e^{-j\phi_{m,l}}, \quad (2)$$

where $m \in \mathbb{Z}_{M_x}$, $l \in \mathbb{Z}_{M_y}$, $i = \lfloor \frac{m}{Q_x} \rfloor$, $j = \lfloor \frac{l}{Q_y} \rfloor$. Note that “ $\sqrt{\frac{1}{Q_x Q_y}}$ ” results from the power divider for upholding the conservation of energy such that

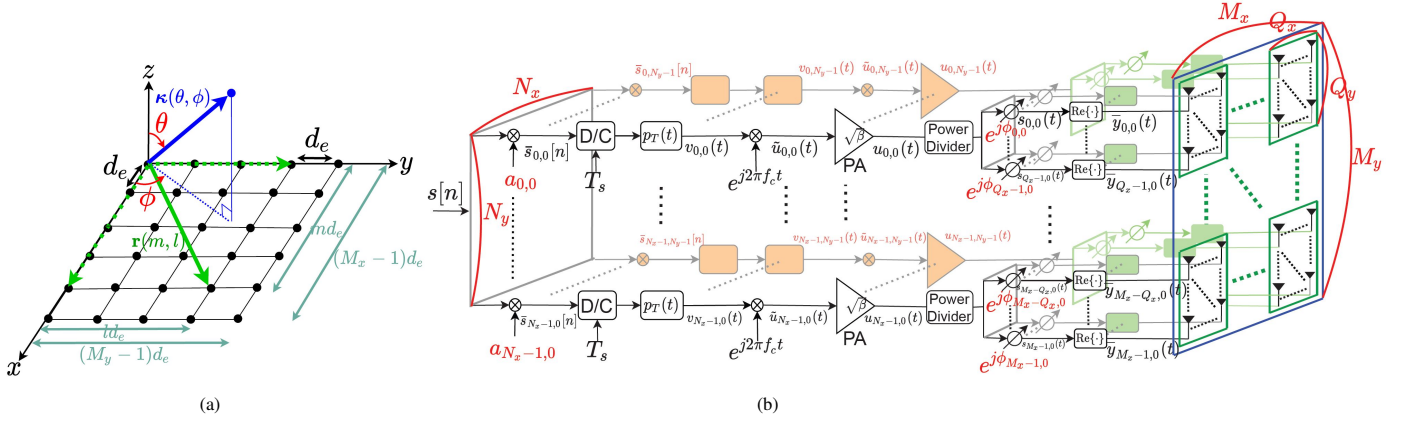


Fig. 1: (a) Uniform Rectangular Array (URA) and (b) SAT Tx hybrid beamforming system model.

$|u_{i,j}(t)|^2 = \sum_{m=i}^{Q_x(i+1)-1} \sum_{l=j}^{Q_y(j+1)-1} |s_{m,l}(t)|^2$. Moreover, the relationship between $a_{i,j}^2$ and $|\mathbf{W}_{m,l}|^2$ is

$$a_{i,j}^2 = \sum_{m=i}^{Q_x(i+1)-1} \sum_{l=j}^{Q_y(j+1)-1} |\mathbf{W}_{m,l}|^2. \quad (3)$$

In Fig. 1b, the transmitted signal of the (m, l) -th antenna can be expressed as

$$\begin{aligned} \bar{y}_{m,l}(t) &= \Re \left\{ \sqrt{\frac{1}{Q_x Q_y}} a_{i,j} e^{j\phi_{m,l}} \sqrt{\beta} e^{j2\pi f_c t} s(t) \right\} \\ &= \Re \left\{ [\mathbf{W}_{m,l}]^* \sqrt{\beta} e^{j2\pi f_c t} s(t) \right\}, \end{aligned} \quad (4)$$

where $s(t) = \sum_{n=-\infty}^{\infty} s[n] p_T(t - nT_s)$. Assume $s(t)$ is narrowband. The signal transmitted from the (m, l) -th antenna will experience propagation delay $\tau_{m,l}(\theta, \phi)$ defined in (1). The signal in far-field (towards the angle (θ, ϕ)) is written as

$$\begin{aligned} y(t) &= \Re \left\{ \sum_{m=0}^{M_x-1} \sum_{l=0}^{M_y-1} \bar{y}_{m,l}(t - \tau_{m,l}(\theta, \phi)) \right\} \\ &= \Re \left\{ \sqrt{\beta} e^{j2\pi f_c t} \sum_{m=0}^{M_x-1} \sum_{l=0}^{M_y-1} [\mathbf{W}_{m,l}]^* e^{-j2\pi f_c \tau_{m,l}(\theta, \phi)} s(t) \right\}. \end{aligned} \quad (5)$$

We define the URA transmit beampattern as [31]

$$\tilde{\mathbf{B}}(\mathbf{W}, \theta, \phi) = \sum_{m=0}^{M_x-1} \sum_{l=0}^{M_y-1} [\mathbf{W}_{m,l}]^* e^{-j2\pi f_c \tau_{m,l}(\theta, \phi)}, \quad (6)$$

where \mathbf{W} is the URA beamforming coefficient matrix defined in (2), and $\tau_{m,l}(\theta, \phi)$ is the propagation delay defined in (1). Let the distance between the SAT and the UT be $d(\theta)$, and the path loss in SAT downlink be $L(\theta)$ which will be defined in (19). The channel is modeled as

$$h(t) = \frac{1}{\sqrt{L(\theta)}} \delta \left(t - \frac{d(\theta)}{c} \right), \quad (7)$$

where c is the speed of light. In Fig. 2, UT Rx is shown. The received signal is $y_r(t) = (y * h)(t) = \frac{1}{\sqrt{L(\theta)}} y \left(t - \frac{d(\theta)}{c} \right)$, and its pre-envelope is expressed as

$$\begin{aligned} \tilde{y}(t) &= y_r(t) + j\hat{y}_r(t) \\ &= \sqrt{\frac{\beta}{L(\theta)}} e^{j2\pi f_c \left(t - \frac{d(\theta)}{c} \right)} \tilde{\mathbf{B}}(\mathbf{W}, \theta, \phi) s \left(t - \frac{d(\theta)}{c} \right), \end{aligned} \quad (8)$$

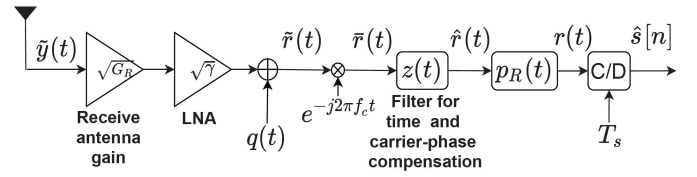


Fig. 2: UT Rx system model.

where $\hat{y}_r(t)$ is the Hilbert transform of $y_r(t)$ [32]. Let G_R be the receive antenna gain and γ be the gain factor of the low noise amplifier (LNA). The noise is modeled as $q(t) = \sqrt{\gamma} q_a(t) + q_\gamma(t)$ [33], where $q_a(t)$ is the amount of noise that enters the antenna and $q_\gamma(t)$ is the noise introduced by the LNA. $q_a(t) \sim \mathcal{N}(0, \frac{kT_a}{2})$ is modeled as a zero-mean additive white Gaussian noise (AWGN) with variance $\frac{kT_a}{2}$, where T_a [K] is the antenna temperature [34] and $k = 1.38 \times 10^{-23}$ [W · s/K] is the Boltzmann constant. $q_\gamma(t) \sim \mathcal{N}(0, \frac{kT_\gamma}{2})$, where T_γ [K] is the noise temperature of the LNA. We then have $\tilde{r}(t) = \sqrt{\gamma} G_R \tilde{y}(t) + q(t)$, where $q(t) \sim \mathcal{N}(0, \frac{\gamma k T_a}{2} + \frac{k T_\gamma}{2})$. Let $\tilde{r}(t)$ go through down converter and filter $z(t) = \delta \left(t + \frac{d(\theta)}{c} \right) e^{j2\pi f_c \left(t + \frac{d(\theta)}{c} \right)}$ which aims for compensating time misalignment and carrier phase difference due to the signal propagation delay $\frac{d(\theta)}{c}$ introduced in the channel $h(t)$ defined in (7). We obtain $\hat{r}(t) = (\tilde{r} * z)(t) = \sqrt{\frac{\beta \gamma G_R}{L(\theta)}} \tilde{\mathbf{B}}(\mathbf{W}, \theta, \phi) s(t) + q'(t)$, where $\tilde{r}(t) = \tilde{r}(t) e^{-j2\pi f_c t}$ and $q'(t) = (q(t) e^{-j2\pi f_c t}) * z(t)$. If the gain of the first amplifying stage is large, noises introduced by the subsequent components have a diminishing effect on the SNR according to the Friis formula [34]. Since γ is typically a large value, the noise introduced by other components is considered negligible for convenience. Apply the receiving filter $p_R(t)$, we get $r(t) = (\hat{r} * p_R)(t)$. Suppose Nyquist pulse-shaping criterion for zero ISI is met (i.e., $(p_T * p_R)(nT_s) = \delta[n]$ [32]). The received discrete-time signal is derived as

$$\hat{s}[n] = \sqrt{\frac{\beta \gamma G_R}{L(\theta)}} \tilde{\mathbf{B}}(\mathbf{W}, \theta, \phi) s[n] + q[n]. \quad (9)$$

The baseband equivalent noise $q[n] \sim \mathcal{CN}(0, \gamma k T_{\text{sys}} f_{\text{BW}})$ is a zero-mean circularly symmetric Gaussian noise with

variance $\gamma k T_{\text{sys}} f_{\text{BW}}$ [5], where f_{BW} [Hz] is the channel bandwidth, and the system noise temperature is defined as $T_{\text{sys}} [\text{K}] = T_a [\text{K}] + T_e [\text{K}]$ [34], where T_a is the antenna temperature and T_e is the effective noise temperature. Since we only consider the noise introduced by LNA, $T_e = \frac{T_\gamma}{\gamma}$ in our case. Given the noise factor N_f [dB], one can calculate $T_e = (10^{0.1N_f} [\text{dB}] - 1)T_0$, where $T_0 = 290 [\text{K}]$ is the standard temperature [34].

C. Baseband Equivalent Transceiver Model

According to (9), the baseband transceiver models with hybrid and fully digital beamforming structures are depicted in Fig. 3a and Fig. 3b, respectively. In both Fig. 3a and Fig. 3b, $\tilde{y}[n] = \sqrt{\beta} \tilde{\mathbf{B}}(\mathbf{W}, \theta, \phi) s[n]$, and $\hat{s}[n] = \sqrt{\frac{\gamma G_R}{L(\theta)}} \tilde{y}[n] + q[n] = \sqrt{\frac{\beta \gamma G_R}{L(\theta)}} \tilde{\mathbf{B}}(\mathbf{W}, \theta, \phi) s[n] + q[n]$ as derived in (9). In Fig. 3a, PA average output power can be computed as $\forall i \in \mathbb{Z}_{N_x}, j \in \mathbb{Z}_{N_y}$

$$P_{\text{PA,avg}}^{(i,j)} = \frac{\mathbb{E}\{|u_{i,j}[n]|^2\}}{R} = \beta P_s a_{i,j}^2 = \beta P_s \sum_{m=iQ_x}^{Q_x(i+1)-1} \sum_{l=jQ_y}^{Q_y(j+1)-1} |[\mathbf{W}]_{m,l}|^2, \quad (10)$$

where $u_{i,j}[n] = \sqrt{\beta} a_{i,j} s[n]$ is the PA output signal, $R = 50 [\Omega]$ is the antenna impedance, the source signal power is

$$P_s = \frac{\mathbb{E}\{|s[n]|^2\}}{R} [\text{W}], \quad (11)$$

and the relationship between $a_{i,j}^2$ and $|\mathbf{W}_{m,l}|^2$ is shown in (3). Moreover, transmit signal power is the summation of PA average output power in RF chains:

$$P_T = \sum_{i=0}^{N_x-1} \sum_{j=0}^{N_y-1} P_{\text{PA,avg}}^{(i,j)}. \quad (12)$$

III. PROBLEM FORMULATION FOR BROADENED-BEAM URA COEFFICIENT DESIGN IN LEO SATCOMS

A. LEO SatComs Scenario

A scenario of LEO SatComs is illustrated in Fig. 4a. The coordinate system (x, y, z) is defined from the SAT perspective, where the z axis represents the direction from SAT toward the center of the Earth. Assume the SAT is at altitude h with SAT elevation angle, $\theta \in [0, \frac{\pi}{2}]$, and SAT azimuth angle, $\phi \in [0, 2\pi]$. Suppose that the transmit beamformer described in Section II is mounted on the SAT for communication. Let SAT service angle be θ_{svc} , and SAT field of view (FoV) angle θ_e be the angle between z -axis and the SAT to the Earth's tangent point. From $\triangle OSE$ in Fig. 4b, SAT FoV angle can be calculated as

$$\theta_e = \sin^{-1} \left(\frac{R_e}{h + R_e} \right), \quad (13)$$

where R_e is the Earth's radius. We regard $\theta \in [\theta_e, \frac{\pi}{2}]$ as the "don't care" angle region since the transmitted signals within the region would not reach the Earth. Transmit beampattern main lobe angle set is defined as

$$\Pi_m = \{(\theta, \phi) | \theta \in [0, \theta_{\text{svc}}], \phi \in [0, 2\pi]\}, \quad (14)$$

and SAT service areas correspond to the orange-colored areas in Fig 4a. Transmit beampattern sidelobe angle set is defined as

$$\Pi_s = \{(\theta, \phi) | \theta \in [\theta_s, \theta_e], \phi \in [0, 2\pi]\}, \quad (15)$$

and SAT out-of-beam areas correspond to the blue-colored areas in Fig 4a. Let the distance between SAT and the ground UT be $d(\theta)$. From $\triangle OSB$ in Fig. 4b, according to law of cosines, we have $R_E^2 = d(\theta)^2 + (h + R_e)^2 - 2d(\theta)(h + R_e) \cos(\theta)$. Then $d(\theta)$, $\forall \theta \in [0, \theta_e]$, is obtained as

$$d(\theta) = (h + R_e) \cos(\theta) - \sqrt{R_E^2 - (h + R_e)^2 \sin^2(\theta)}. \quad (16)$$

Also, SAT service areas, A_{svc} , are areas of the spherical cap in Fig. 4b which can be calculated by [35]

$$A_{\text{svc}} = 2\pi R_e^2 (1 - \cos(\varphi)), \quad (17)$$

where

$$\varphi = \pi - \theta - \zeta, \quad \theta \in [0, \theta_e], \quad (18)$$

and $\zeta = \pi - \sin^{-1} \left(\frac{R_e + h}{R_e} \sin(\theta) \right) \in [\frac{\pi}{2}, \pi]$ is obtained by the law of sines $\frac{R_e}{\sin(\theta)} = \frac{R_e + h}{\sin(\zeta)}$.

B. Received SNR Derivation

In the SAT downlink, signal strength is degraded due to transmission loss $L(\theta)$, including Tx cable loss $L_{c,T}$, Rx cable loss $L_{c,R}$, atmospheric path loss L_a , scintillation loss L_{sl} , and free-space propagation loss $L_{\text{fs}}(\theta)$. The transmission loss is considered as [36]

$$L(\theta) = L_{c,T} L_{c,R} L_{\text{fs}}(\theta) L_a L_{\text{sm}} L_{\text{sl}} = \sigma^2(\theta) L_0, \quad (19)$$

where $L_{\text{fs}}(\theta) = \left(\frac{4\pi d(\theta)}{\lambda} \right)^2$ with $d(\theta)$ derived in (16), λ is the wavelength of the transmitted signal,

$$L_0 = L_{c,T} L_{c,R} L_a L_{\text{sm}} L_{\text{sl}} \left(\frac{4\pi h}{\lambda} \right)^2, \quad (20)$$

$$\sigma(\theta) = \frac{d(\theta)}{h} = \frac{(h + R_e) \cos(\theta) - \sqrt{R_E^2 - (h + R_e)^2 \sin^2(\theta)}}{h}. \quad (21)$$

Note that $\sigma : [0, \theta_e] \rightarrow \mathbb{R}$ with θ_e defined in (13). In Fig. 5a, $\sigma(\theta)$ is depicted.

According to the received discrete-time signal $\hat{s}[n]$ derived in (9), the received signal power can be calculated as

$$P_r(\mathbf{W}, \theta, \phi) = \frac{\mathbb{E}\{|s_r[n]|^2\}}{R} = \left(\frac{\beta \gamma G_R}{\sigma^2(\theta) L_0} \right) P_s |\tilde{\mathbf{B}}(\mathbf{W}, \theta, \phi)|^2, \quad (22)$$

where $s_r[n] = \sqrt{\frac{\beta \gamma G_R}{L(\theta)}} \tilde{\mathbf{B}}(\mathbf{W}, \theta, \phi) s[n]$, $R = 50 [\Omega]$ is the antenna impedance, and P_s is defined in (11). Also, since the baseband noise derived in (9) is $q[n] \sim \mathcal{CN}(0, \gamma k T_{\text{sys}} f_{\text{BW}})$, the noise power is evaluated as [5], [34]

$$P_N = \gamma k T_{\text{sys}} f_{\text{BW}}, \quad (23)$$

where $k = 1.39 \times 10^{-23} [\text{W} \cdot \text{s}/\text{K}]$ is the Boltzmann constant, f_{BW} [Hz] is the channel bandwidth, and T_{sys} [K] is the system noise temperature. The received SNR can be derived as

$$\text{SNR}(\mathbf{W}, \theta, \phi) = \frac{P_r(\mathbf{W}, \theta, \phi)}{P_N} = \frac{\beta G_R P_s |\tilde{\mathbf{B}}(\mathbf{W}, \theta, \phi)|^2}{\sigma^2(\theta) L_0 k T_{\text{sys}} f_{\text{BW}}}. \quad (24)$$

In (24), the ratio of G_R and T_{sys} is typically referred to as the antenna gain-to-noise-temperature G/T [dB/K] = $10 \log_{10} \left(\frac{G_R}{T_{\text{sys}}} \right)$ [36].

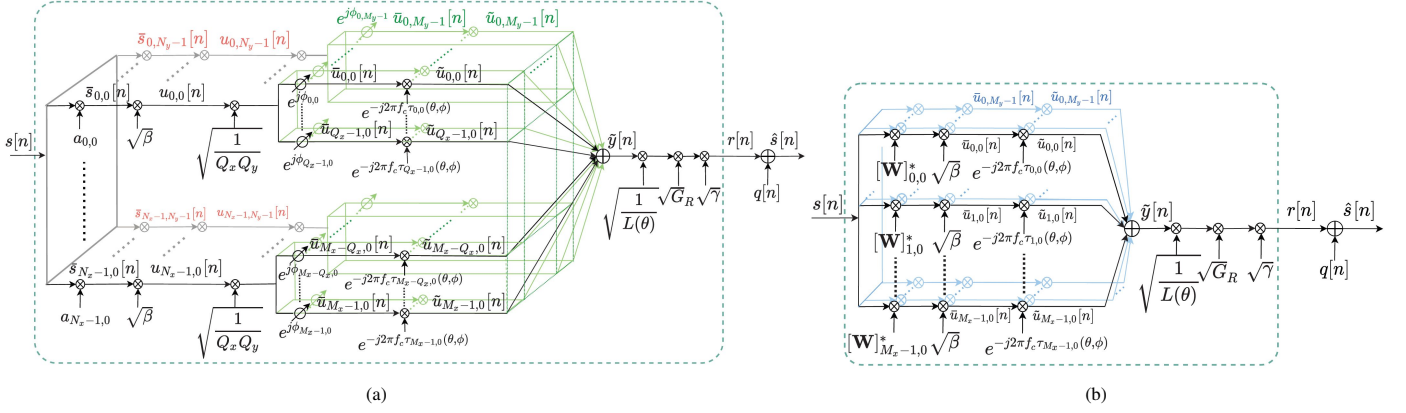


Fig. 3: (a) Baseband transceiver model with (a) hybrid beamforming structure and (b) fully digital beamforming structure.

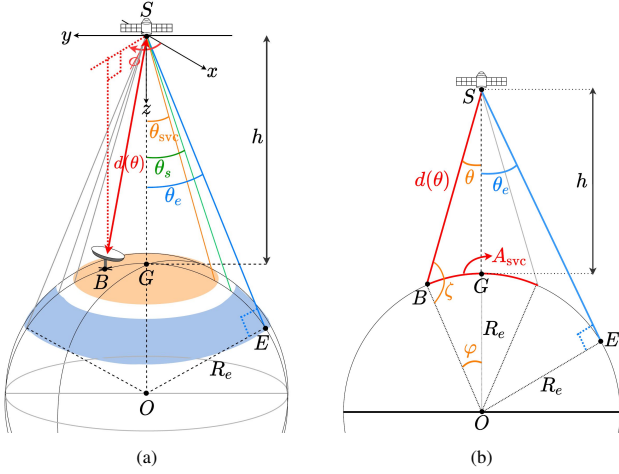


Fig. 4: (a) A LEO SatComs scenario and (b) Side view of (a) for calculating SAT FoV angle θ_e , the distance between SAT and UT $d(\theta)$, and SAT service areas A_{svc} .

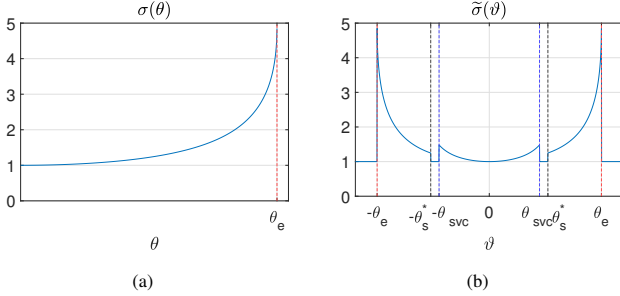


Fig. 5: (a) $\sigma(\theta)$ defined in (21) and (b) $\tilde{\sigma}(\vartheta)$ defined in (38).

C. Problem Formulation

An optimization problem for URA coefficient design in LEO SatComs under QoS and constant modulus constraints is formulated in (25). The objective function (25a) aims to suppress the maximum received signal power in SAT out-of-beam areas to mitigate interference. The QoS in SAT service areas is guaranteed by (25b), and CMC is considered in (25c).

$$\underset{\mathbf{W} \in \mathbb{C}^{M_x \times M_y}}{\text{minimize}} \quad \sup_{\forall(\theta, \phi) \in \Pi_s} P_r(\mathbf{W}, \theta, \phi) \quad (25a)$$

$$\text{subject to} \quad \text{SNR}(\mathbf{W}, \theta, \phi) \geq \text{SNR}_{\min}, \forall(\theta, \phi) \in \Pi_m \quad (25b)$$

$$|[\mathbf{W}]_{m,l}| = 1, m \in \mathbb{Z}_{M_x}, l \in \mathbb{Z}_{M_y}, \quad (25c)$$

where the $P_r(\mathbf{W}, \theta, \phi)$ is derived in (22), $\text{SNR}(\mathbf{W}, \theta, \phi)$ is derived in (24), SNR_{\min} is the received SNR lower bound in SAT service areas which will be set in Table II, Π_m is the transmit beampattern main lobe angle set defined in (14) with specified SAT service angle θ_{svc} , and Π_s is the transmit beampattern sidelobe angle set defined in (15). We can reformulate the problem (25) as its epigraph representation

$$\underset{\mathbf{W} \in \mathbb{C}^{M_x \times M_y}, t \in \mathbb{R}_+}{\text{minimize}} \quad t^2 \quad (26a)$$

$$\text{subject to} \quad P_r(\mathbf{W}, \theta, \phi) \leq t^2, \forall(\theta, \phi) \in \Pi_s \quad (26b)$$

$$\text{SNR}(\mathbf{W}, \theta, \phi) \geq \text{SNR}_{\min}, \forall(\theta, \phi) \in \Pi_m \quad (26c)$$

$$|[\mathbf{W}]_{m,l}| = 1, m \in \mathbb{Z}_{M_x}, l \in \mathbb{Z}_{M_y}. \quad (26d)$$

Based on $P_r(\mathbf{W}, \theta, \phi)$ derived in (22) and $\text{SNR}(\mathbf{W}, \theta, \phi)$ derived in (24), the problem (26) can be transferred to the following equivalent problem

$$\underset{\mathbf{W} \in \mathbb{C}^{M_x \times M_y}, t \in \mathbb{R}_+}{\text{minimize}} \quad t \quad (27a)$$

$$\text{subject to} \quad |\tilde{\mathbf{B}}(\mathbf{W}, \theta, \phi)| \leq t\sigma(\theta), \forall(\theta, \phi) \in \Pi_s \quad (27b)$$

$$|\tilde{\mathbf{B}}(\mathbf{W}, \theta, \phi)| \geq \alpha\sigma(\theta), \forall(\theta, \phi) \in \Pi_m \quad (27c)$$

$$|[\mathbf{W}]_{m,l}| = 1, m \in \mathbb{Z}_{M_x}, l \in \mathbb{Z}_{M_y}, \quad (27d)$$

where $\sigma(\theta)$ is defined in (21) and

$$\alpha = \sqrt{\frac{\text{SNR}_{\min} k T_{\text{sys}} f_{\text{BW}} L_0}{\beta G_R P_s}}. \quad (28)$$

We can observe that the QoS guarantee constraint (25b) results in the beampattern main lobe lower bound constraint (27c), and the main lobe lower bound is anticipated to follow the shape of $\sigma(\theta)$ as shown in Fig. 5a. The shape of $\sigma(\theta)$ is related to the distance variation between SAT and UT due to the Earth's curvature which has also been considered in [9]–[13] for synthesizing the isoflux radiation patterns. Different from [9]–[13] that aims to synthesize isoflux radiation patterns without main lobe variation, we only constrain the main lobe lower bound to guarantee the received SNR in SAT service areas. We suppose that each UT can select proper modulation and coding schemes (MODCODs) based on the received SNR for decoding. Hence, there is no need to constrain all UTs for having the same received SNR, and we don't have to put strict constraints for synthesizing patterns without main lobe

variation. Moreover, we consider CMC (25c) which has not been considered in [9]–[13].

IV. PROPOSED METHOD

A. Idea of URA Design Problem Decomposition

URA with a large number of antenna elements, e.g., 32×32 , is preferable for SATs to enhance downlink capacity. However, it requires intensive computations to directly solve the URA design problem (27) when variable \mathbf{W} has a large size. To mitigate the complexity of designing a URA, we propose to decompose a URA design problem into ULA design problems with the idea of Kronecker product beamforming [28]–[31]. If we have separable weightings

$$\mathbf{W} = \mathbf{x}\mathbf{y}^T \in \mathbb{C}^{M_x \times M_y}, \quad (29)$$

where $\mathbf{x} \in \mathbb{C}^{M_x}$ and $\mathbf{y} \in \mathbb{C}^{M_y}$, or equivalently expressed with the Kronecker product property $\text{vec}(\mathbf{W}) = \mathbf{x} \otimes \mathbf{y}$, the URA beampattern defined in (6) can be derived as the product of two ULA beampatterns [28], [31],

$$\begin{aligned} \tilde{\mathbf{B}}(\mathbf{W}, \theta, \phi) &= \sum_{m=0}^{M_x-1} \sum_{l=0}^{M_y-1} [\mathbf{W}]_{m,l}^* e^{-j2\pi f_c \bar{\tau}_{m,l}(\theta, \phi)} \\ &= \sum_{m=0}^{M_x-1} x_m^* e^{-j2\pi f_c \bar{\tau}_m(\vartheta_x)} \sum_{l=0}^{M_y-1} y_l^* e^{-j2\pi f_c \bar{\tau}_l(\vartheta_y)} \\ &= \mathbf{B}(\mathbf{x}, \vartheta_x) \mathbf{B}(\mathbf{y}, \vartheta_y), \end{aligned} \quad (30)$$

where

$$\vartheta_x = \sin^{-1}(\sin(\theta) \cos(\phi)), \quad \vartheta_y = \sin^{-1}(\sin(\theta) \sin(\phi)), \quad (31)$$

and $\mathbf{B}(\mathbf{x}, \vartheta)$ is the ULA beampattern defined as [31]

$$\mathbf{B}(\mathbf{x}, \vartheta) = \mathbf{x}^H \mathbf{a}(\vartheta) = \sum_{m=0}^{M_x-1} x_m^* e^{-j2\pi f_c \bar{\tau}_m(\vartheta)}, \quad (32)$$

where $\bar{\tau}_m(\vartheta) = \frac{md_e \sin(\vartheta)}{c}$, $\forall \vartheta \in [-\frac{\pi}{2}, \frac{\pi}{2}]$, and $\mathbf{x} = [x_0, \dots, x_{M_x-1}]^T$, $\mathbf{a}(\vartheta) = [1, \dots, e^{-j2\pi f_c \bar{\tau}_{M_x-1}(\vartheta)}]^T$.

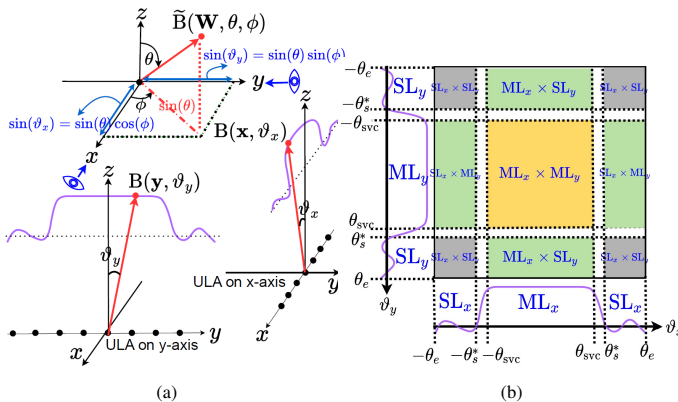


Fig. 6: (a) Visualization of the “composite” URA beampattern based on (30) and (b) Components of the “composite” URA beampattern (ML_x/ML_y and SL_x/SL_y represent the main lobe/sidelobe region of ULA beampattern with respect to ϑ_x/ϑ_y axis).

Based on (30), the URA beampattern, $\tilde{\mathbf{B}}(\mathbf{W}, \theta, \phi)$, can be composed of two ULA beampatterns, $\mathbf{B}(\mathbf{x}, \vartheta_x)$ and $\mathbf{B}(\mathbf{y}, \vartheta_y)$, which are generated by the ULAs placed on x/y -axis as depicted in Fig. 6a. For convenience, we name the URA beampattern generated through (30) as the “composite” URA beampattern. In Fig. 6b, the expected components of the

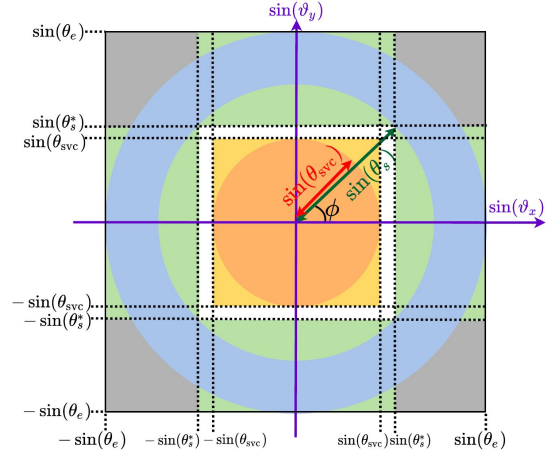


Fig. 7: Top view of the “composite” URA beampattern. (Orange and blue annular ring areas are the expected URA beampattern main lobe and sidelobe region in the problem (27). Yellow areas correspond to the main lobe region of the “composite” URA beampattern; while, green and gray areas correspond to its sidelobe region.)

“composite” URA beampattern are illustrated. Its main lobe region is highlighted in yellow square which are composed of the ULA beampatterns’ main lobe region. While, green and gray-colored areas are sidelobe regions of the “composite” URA beampattern. Note that the expected main lobe/sidelobe region of the “composite” URA beampattern are different from that in the URA design problem (27). In the problem (27), with the main lobe angle set Π_m defined in (14), the expected URA beampattern main lobe region corresponds to the orange-colored circle in Fig. 7. While, with the sidelobe angle set Π_s defined in (15), the expected URA beampattern sidelobe region corresponds to the blue-colored annular ring in Fig. 7. To ensure the main lobe/sidelobe region of the “composite” URA beampattern contains the expected URA beampattern main lobe/sidelobe region in the problem (27), the ULA main lobe angle set in the problem (39) is defined as

$$\Theta_m = [-\theta_{\text{svc}}, \theta_{\text{svc}}]. \quad (33)$$

The ULA sidelobe angle set in the problem (39) is defined as

$$\Theta_s = [-\theta_e, -\theta_s^*] \cup [\theta_s^*, \theta_e], \quad (34)$$

where

$$\theta_s^* = \sin^{-1} \left(\frac{\sin(\theta_s)}{\sqrt{2}} \right). \quad (35)$$

Also, we restrict $\theta_{\text{svc}} \leq \sin^{-1} \left(\frac{\sin(\theta_s)}{\sqrt{2}} \right)$ to prevent the “composite” URA beampattern main lobe region (i.e., yellow-colored square in Fig. 7) from overlapping the sidelobe region expected in the problem (27) (i.e., blue-colored annular ring in Fig. 7).

Furthermore, $\sigma(\theta)$ defined in (21) needs to be modified for formulating the problem (39). Firstly, inequalities in (36) is a sufficient condition of the constraint (27b).

$$|\mathbf{B}(\mathbf{x}, \vartheta_x)| \leq \sqrt{t\bar{\sigma}(\vartheta_x)}, \quad \forall \vartheta_x \in \Theta_s, \quad (36a)$$

$$|\mathbf{B}(\mathbf{y}, \vartheta_y)| \leq \sqrt{t\bar{\sigma}(\vartheta_y)}, \quad \forall \vartheta_y \in \Theta_s, \quad (36b)$$

$$\sqrt{\bar{\sigma}(\vartheta_x)\bar{\sigma}(\vartheta_y)} \leq \sigma(\theta), \quad \forall \vartheta_x, \vartheta_y \in \Theta_s, \forall \theta \in [\theta_s, \theta_e], \quad (36c)$$

such that $|\tilde{\mathbf{B}}(\mathbf{W}, \theta, \phi)| = |\mathbf{B}(\mathbf{x}, \vartheta_x)| |\mathbf{B}(\mathbf{y}, \vartheta_y)| \leq t\sigma(\theta)$. To satisfy (36c), we can select $\bar{\sigma}(\vartheta_x) = \sigma(\vartheta_x)$, $\bar{\sigma}(\vartheta_y) = \sigma(\vartheta_y)$,

$\forall \vartheta_x, \vartheta_y \in \Theta_s$. To show that the selection meets (36c), we have $\forall \vartheta_x \in \Theta_s$:

$$\tilde{\sigma}(\vartheta_x) = \sigma(\vartheta_x) \stackrel{(a)}{=} \sigma(\sin^{-1}(\sin(\theta) \cos(\phi))) \stackrel{(b)}{\leq} \sigma(\sin^{-1}(\sin(\theta))) = \sigma(\theta),$$

where (a) holds by (31), and (b) holds since both $\sigma(\theta)$ and $\sin^{-1}(\theta)$ are non-decreasing functions $\forall \theta \in (0, \theta_e)$. Similarly, it can be shown that $\tilde{\sigma}(\vartheta_y) = \sigma(\vartheta_y) \leq \sigma(\theta)$. Secondly, inequalities in (37) is a sufficient condition of the constraint (27c).

$$|\mathbf{B}(\mathbf{x}, \vartheta_x)| \geq \sqrt{\alpha \tilde{\sigma}(\vartheta_x)}, \quad \forall \vartheta_x \in \Theta_m, \quad (37a)$$

$$|\mathbf{B}(\mathbf{y}, \vartheta_y)| \geq \sqrt{\alpha \tilde{\sigma}(\vartheta_y)}, \quad \forall \vartheta_y \in \Theta_m, \quad (37b)$$

$$\sqrt{\tilde{\sigma}(\vartheta_x) \tilde{\sigma}(\vartheta_y)} \geq \sigma(\theta), \quad \forall \vartheta_x, \vartheta_y \in \Theta_m, \quad \forall \theta \in [0, \theta_{\text{svc}}], \quad (37c)$$

such that $|\tilde{\mathbf{B}}(\mathbf{W}, \theta, \phi)| = |\mathbf{B}(\mathbf{x}, \vartheta_x)| |\mathbf{B}(\mathbf{y}, \vartheta_y)| \geq \alpha \sigma(\theta)$. To satisfy (37c), we can select $\tilde{\sigma}(\vartheta_x) = \tilde{\sigma}(\vartheta_y) = \sigma(\theta)$, $\forall \vartheta_x, \vartheta_y \in \Theta_m$, $\forall \theta \in [0, \theta_{\text{svc}}]$. By the relationship $\sin(\theta) = \sqrt{2} \sin(\vartheta_x) = \sqrt{2} \sin(\vartheta_y)$, we can choose $\tilde{\sigma}(\vartheta_x) = \sigma(\theta)|_{\theta=\sin^{-1}(\sqrt{2} \sin(\vartheta_x))}$, $\tilde{\sigma}(\vartheta_y) = \sigma(\theta)|_{\theta=\sin^{-1}(\sqrt{2} \sin(\vartheta_y))}$, $\forall \vartheta_x, \vartheta_y \in \Theta_m$. As a result, $\tilde{\sigma}: [-\theta_e, \theta_e] \rightarrow \mathbb{R}$, plotted in Fig. 5b, is defined as

$$\tilde{\sigma}(\vartheta) = \begin{cases} \sigma(\theta)|_{\theta=\sin^{-1}(\sqrt{2} \sin(\vartheta))}, & \vartheta \in \Theta_m = [-\theta_{\text{svc}}, \theta_{\text{svc}}], \theta_{\text{svc}} \leq \frac{\pi}{4} \\ \sigma(\vartheta), & \vartheta \in \Theta_s = [-\theta_e, -\theta_s^*] \cup [\theta_s^*, \theta_e] \\ 1, & \text{else.} \end{cases} \quad (38)$$

B. Problem Reformulation of URA Design Problem (27) to ULA Design Subproblems

Combining (30), (36) and (37), the URA design problem (27) is transferred to

$$\underset{\mathbf{x} \in \mathbb{C}^{M_x}, \mathbf{y} \in \mathbb{C}^{M_y}, t \in \mathbb{R}_+}{\text{minimize}} \quad t \quad (39a)$$

$$\text{subject to } |\mathbf{B}(\mathbf{x}, \vartheta_x)| |\mathbf{B}(\mathbf{y}, \vartheta_y)| \leq t \sqrt{\tilde{\sigma}(\vartheta_x) \tilde{\sigma}(\vartheta_y)}, \quad \forall \vartheta_x, \vartheta_y \in \Theta_s \quad (39b)$$

$$|\mathbf{B}(\mathbf{x}, \vartheta_x)| |\mathbf{B}(\mathbf{y}, \vartheta_y)| \geq \alpha \sqrt{\tilde{\sigma}(\vartheta_x) \tilde{\sigma}(\vartheta_y)}, \quad \forall \vartheta_x, \vartheta_y \in \Theta_m \quad (39c)$$

$$|x_m| |y_l| = 1, \quad m \in \mathbb{Z}_{M_x}, l \in \mathbb{Z}_{M_y}, \quad (39d)$$

where $\tilde{\sigma}(\vartheta)$ is defined in (38). We then decompose the problem (39) into two identical ULA design subproblems (40) and (41),

$$\underset{\mathbf{x} \in \mathbb{C}^{M_x}, t \in \mathbb{R}_+}{\text{minimize}} \quad t \quad (40a)$$

$$\text{subject to } |\mathbf{B}(\mathbf{x}, \vartheta_x)| \leq \sqrt{t \tilde{\sigma}(\vartheta_x)}, \quad \forall \vartheta_x \in \Theta_s \quad (40b)$$

$$|\mathbf{B}(\mathbf{x}, \vartheta_x)| \geq \sqrt{\alpha \tilde{\sigma}(\vartheta_x)}, \quad \forall \vartheta_x \in \Theta_m \quad (40c)$$

$$|x_m| = 1, \quad m \in \mathbb{Z}_{M_x}. \quad (40d)$$

$$\underset{\mathbf{y} \in \mathbb{C}^{M_y}, t \in \mathbb{R}_+}{\text{minimize}} \quad t \quad (41a)$$

$$\text{subject to } |\mathbf{B}(\mathbf{y}, \vartheta_y)| \leq \sqrt{t \tilde{\sigma}(\vartheta_y)}, \quad \forall \vartheta_y \in \Theta_s \quad (41b)$$

$$|\mathbf{B}(\mathbf{y}, \vartheta_y)| \geq \sqrt{\alpha \tilde{\sigma}(\vartheta_y)}, \quad \forall \vartheta_y \in \Theta_m \quad (41c)$$

$$|y_m| = 1, \quad m \in \mathbb{Z}_{M_y}. \quad (41d)$$

Since the two subproblems (40) and (41) are identical, we will only demonstrate the method to solve the subproblem (40).

The quadratic form of the problem (40) can be obtained as

$$\underset{\mathbf{x} \in \mathbb{C}^{M_x}, t \in \mathbb{R}_+}{\text{minimize}} \quad t \quad (42a)$$

$$\text{subject to } \mathbf{x}^H \mathbf{A}(\vartheta_x) \mathbf{x} \leq t \tilde{\sigma}(\vartheta), \quad \forall \vartheta_x \in \Theta_s \quad (42b)$$

$$\mathbf{x}^H \mathbf{A}(\vartheta_x) \mathbf{x} \geq \alpha \tilde{\sigma}(\vartheta), \quad \forall \vartheta_x \in \Theta_m \quad (42c)$$

$$\mathbf{x}^H \mathbf{E}_m \mathbf{x} = 1, \quad m \in \mathbb{Z}_{M_x}, \quad (42d)$$

where $\mathbf{A}(\vartheta) = \mathbf{a}(\vartheta) \mathbf{a}^H(\vartheta)$, $\mathbf{E}_m = \mathbf{e}_m \mathbf{e}_m^H$, and \mathbf{e}_m is the m -th M_x -dimensional standard vector. Uniformly sampled the main lobe angle set Θ_m by δ with N_{svc} points, we have $\vartheta_i = -\theta_{\text{svc}} + \delta \cdot i$ for $i \in \mathbb{Z}_{N_{\text{svc}}}$ with $N_{\text{svc}} = \frac{2\theta_{\text{svc}}}{\delta} + 1$. Also, uniformly sampled the sidelobe angle set Θ_s by δ with N_s points, we have $\vartheta_k = -\theta_e + \delta \cdot k$; $k \in \{0, \dots, \frac{\theta_e - \theta_s^*}{\delta}\}$ and $\vartheta_k = \theta_s^* + \delta \cdot (k - \frac{\theta_e - \theta_s^*}{\delta} - 1)$; $k \in \{\frac{\theta_e - \theta_s^*}{\delta} + 1, \dots, N_s - 1\}$ with $N_s = 2(\frac{\theta_e - \theta_s^*}{\delta} + 1)$. Define $\mathbf{X} = \mathbf{x} \mathbf{x}^H$, then the problem we intend to solve becomes

$$\underset{\mathbf{X} \in \mathbb{H}_+^{M_x}, t \in \mathbb{R}_+}{\text{minimize}} \quad t \quad (43a)$$

$$\text{subject to } \text{Tr}(\mathbf{X} \mathbf{A}(\vartheta_k)) \leq t \tilde{\sigma}(\vartheta_k), \quad \forall k \in \mathbb{Z}_{N_s} \quad (43b)$$

$$\text{Tr}(\mathbf{X} \mathbf{A}(\vartheta_i)) \geq \alpha \tilde{\sigma}(\vartheta_i), \quad \forall i \in \mathbb{Z}_{N_{\text{svc}}} \quad (43c)$$

$$\text{Tr}(\mathbf{X} \mathbf{E}_m) = 1, \quad m \in \mathbb{Z}_{M_x} \quad (43d)$$

$$\text{rank}(\mathbf{X}) = 1. \quad (43e)$$

Note that problem (43) is a non-convex optimization problem due to the rank-1 constraint (43e).

C. Proposed Algorithm

A convex iterative algorithm is proposed in Algorithm 1 to address the non-convex optimization problem (43). To obtain the rank-1 matrix \mathbf{X} , the concept of the algorithm is to suppress the sum of the second largest eigenvalue to the smallest eigenvalue in each iteration until the ratio of the largest eigenvalue to the second largest eigenvalue is smaller than the threshold $\varepsilon_{\text{rank}}$. In the $(\psi - 1)$ -th iteration, eigendecomposition of $\mathbf{X}^{(\psi-1)}$ is performed:

$$\mathbf{X}^{(\psi-1)} = \tilde{\mathbf{U}}^{(\psi-1)} \mathbf{D}^{(\psi-1)} (\tilde{\mathbf{U}}^{(\psi-1)})^H, \quad (44)$$

$$\tilde{\mathbf{U}}^{(\psi-1)} = [\mathbf{u}_0^{(\psi-1)}, \dots, \mathbf{u}_{M_x-1}^{(\psi-1)}], \quad (45)$$

$$\mathbf{D}^{(\psi-1)} = \text{diag}(\Lambda_0^{(\psi-1)}, \dots, \Lambda_{M_x-1}^{(\psi-1)}), \quad (46)$$

and $\mathbf{u}_m^{(\psi-1)}$ are the eigenvectors of $\tilde{\mathbf{U}}^{(\psi-1)}$ corresponding to eigenvalues $\Lambda_m^{(\psi-1)}$ in non-increasing order. Let $\mathbf{U}^{(\psi-1)} = [\mathbf{u}_1^{(\psi-1)}, \dots, \mathbf{u}_{M_x-1}^{(\psi-1)}]$ and set

$$\mathbf{V}^{(\psi-1)} = \mathbf{U}^{(\psi-1)} (\mathbf{U}^{(\psi-1)})^H \quad (47)$$

which can be viewed as the unfavorable direction in vector space $\mathbb{H}_+^{M_x}$. The penalty function is introduced [37]

$$\text{Tr}(\mathbf{X}^{(\psi)} \mathbf{V}^{(\psi-1)}). \quad (48)$$

In the (ψ) -th iteration, minimize $\text{Tr}(\mathbf{X}^{(\psi)} \mathbf{V}^{(\psi-1)})$ implies suppressing the sum of the second largest eigenvalue to the smallest eigenvalue. The penalty function (48) is applied in (49a) with penalty parameter ρ . In the (ψ) -th iteration, the convex problem (49) is solved.

$$\underset{\mathbf{X}^{(\psi)} \in \mathbb{H}_+^{M_x}, t \in \mathbb{R}_+}{\text{minimize}} \quad t + \rho \text{Tr}(\mathbf{X}^{(\psi)} \mathbf{V}^{(\psi-1)}) \quad (49a)$$

$$\text{subject to } \text{Tr}(\mathbf{X}^{(\psi)} \mathbf{A}(\vartheta_k)) \leq t \tilde{\sigma}(\vartheta_k), \quad \forall k \in \mathbb{Z}_{N_s} \quad (49b)$$

$$\text{Tr}(\mathbf{X}^{(\psi)} \mathbf{A}(\vartheta_i)) \geq \alpha \tilde{\sigma}(\vartheta_i), \quad \forall i \in \mathbb{Z}_{N_{\text{svc}}} \quad (49c)$$

$$\text{Tr}(\mathbf{X}^{(\psi)} \mathbf{E}_m) = 1, \quad m \in \mathbb{Z}_{M_x}. \quad (49d)$$

Similarly, to tackle the non-convex problem (41), the problem (50) is solved in each iteration.

$$\underset{\mathbf{Y}^{(\psi)} \in \mathbb{H}_+^{M_y}, t \in \mathbb{R}_+}{\text{minimize}} \quad t + \rho \text{Tr}(\mathbf{Y}^{(\psi)} \mathbf{V}^{(\psi-1)}) \quad (50a)$$

$$\text{subject to} \quad \text{Tr}(\mathbf{Y}^{(\psi)} \mathbf{A}(\vartheta_k)) \leq t \tilde{\sigma}(\vartheta_k), \quad \forall k \in \mathbb{Z}_{N_s} \quad (50b)$$

$$\text{Tr}(\mathbf{Y}^{(\psi)} \mathbf{A}(\vartheta_i)) \geq \alpha \tilde{\sigma}(\vartheta_i), \quad \forall i \in \mathbb{Z}_{N_{\text{svc}}} \quad (50c)$$

$$\text{Tr}(\mathbf{Y}^{(\psi)} \mathbf{E}_m) = 1, \quad m \in \mathbb{Z}_{M_y}. \quad (50d)$$

To achieve the rank-1 convergence, the penalty parameter is updated depending on the ratio of the largest eigenvalue to the second largest eigenvalue in the consecutive iteration. Given an initial penalty parameter value $\rho^{(0)}$, we update $\rho^{(\psi)}$ as

$$\rho^{(\psi)} = \begin{cases} \rho^{(\psi-1)} \cdot (1+p), & \text{if } \frac{\Lambda_0^{(\psi)}}{\Lambda_1^{(\psi)}} - \frac{\Lambda_0^{(\psi-1)}}{\Lambda_1^{(\psi-1)}} \leq \kappa \\ \rho^{(\psi-1)}, & \text{else,} \end{cases} \quad (51)$$

where κ and p are the preset positive numbers. The pseudocode of the proposed broadened-beam URA coefficient design method is shown in Algorithm 1. Note that the convergence properties of Algorithm 1 can be influenced by the settings of penalty parameter update strategy (51) and the initial point selection $(\mathbf{x}_{\text{init}}, \mathbf{y}_{\text{init}})$ which will be mentioned in Section V-C.

Algorithm 1 Proposed Broadened-beam URA Coefficient Design Method

Input: $M_x, M_y, \theta_{\text{svc}}, \theta_s, \theta_e, N_{\text{svc}}, N_s, \mathbf{x}_{\text{init}}, \mathbf{y}_{\text{init}}, \text{SNR}_{\text{min}}, f_{\text{BW}}, \beta, P_s, L_0, G/T, \rho^{(0)}, p, \kappa, \varepsilon_{\text{rank}}$

Output: \mathbf{Z}_{opt}

- 1: Calculate θ_s^* by (35).
 - 2: Calculate α by (28).
 - 3: **if initial point \mathbf{x}_{init} is available then**
 - 4: $\mathbf{X}^{(0)} = \mathbf{x}_{\text{init}} \mathbf{x}_{\text{init}}^H$.
 - 5: Perform the eigendecomposition $\mathbf{X}^{(0)} = \tilde{\mathbf{U}}^{(0)} \mathbf{D}^{(0)} \tilde{\mathbf{U}}^{(0)H}$.
 - 6: Set $\mathbf{V}^{(0)}$ according to (47).
 - 7: **else**
 - 8: $\mathbf{V}^{(0)} = \mathbf{0}$.
 - 9: **end if**
 - 10: Let $\psi \leftarrow 1$.
 - 11: **repeat**
 - 12: Solve the problem (49) and obtain $\mathbf{X}^{(\psi)}$.
 - 13: Perform the eigendecomposition $\mathbf{X}^{(\psi)} = \tilde{\mathbf{U}}^{(\psi)} \mathbf{D}^{(\psi)} \tilde{\mathbf{U}}^{(\psi)H}$.
 - 14: Let $\Lambda_0^{(\psi)} = [\mathbf{D}^{(\psi)}]_{0,0}$ and $\Lambda_1^{(\psi)} = [\mathbf{D}^{(\psi)}]_{1,1}$.
 - 15: Update $\mathbf{V}^{(\psi)}$ according to (47).
 - 16: Update penalty parameter $\rho^{(\psi)}$ based on (51).
 - 17: $\psi \leftarrow \psi + 1$.
 - 18: **until** $\Lambda_1^{(\psi)} / \Lambda_0^{(\psi)} \leq \varepsilon_{\text{rank}}$
 - 19: Obtain $\mathbf{x}_{\text{opt}} = \sqrt{\Lambda_0^{(\psi)}} \mathbf{u}_0^{(\psi)}$.
 - 20: Solve the problem (50) and obtain \mathbf{y}_{opt} as the procedure from step 3 to step 19.
 - 21: Obtain URA beamforming coefficient by (29): $\mathbf{W}_{\text{opt}} = \mathbf{x}_{\text{opt}} \mathbf{y}_{\text{opt}}^T$.
-

V. NUMERICAL EVALUATION

A. Definition of Evaluation Metrics

The beampatterns obtained through Algorithm 1 feature curved shapes in both main lobe lower bound and sidelobe upper bound due to $\tilde{\sigma}(\vartheta)$ applied in the constraint (49b) and (49c). However, such curved shapes make it not convenient for us to evaluate the peak sidelobe level (PSL). Consequently, when evaluating PSL, we divide ULA beampatterns by $\sqrt{\tilde{\sigma}(\vartheta)}$ to have constant level of main lobe lower bound and sidelobe upper bound. The normalized peak sidelobe level (NPSL) of the ULA beampattern is defined as

$$\text{NPSL}_{\text{ULA}} = 20 \log_{10} \left(\frac{\max_{\vartheta \in \Theta_s} \left\{ |\mathbf{B}(\mathbf{x}, \vartheta)| / \sqrt{\tilde{\sigma}(\vartheta)} \right\}}{\min_{\vartheta \in \Theta_m} \left\{ |\mathbf{B}(\mathbf{x}, \vartheta)| / \sqrt{\tilde{\sigma}(\vartheta)} \right\}} \right), \quad (52)$$

where $\mathbf{B}(\mathbf{x}, \vartheta)$ is defined in (32), Θ_m is defined in (33), Θ_s is defined in (34), and $\tilde{\sigma}(\vartheta)$ is defined in (38). Similarly, the NPSL of the URA beampattern is defined as

$$\text{NPSL}_{\text{URA}} = 20 \log_{10} \left(\frac{\max_{(\theta, \phi) \in \Pi_s} \left\{ |\tilde{\mathbf{B}}(\mathbf{W}, \theta, \phi)| / \sigma(\theta) \right\}}{\min_{(\theta, \phi) \in \Pi_m} \left\{ |\tilde{\mathbf{B}}(\mathbf{W}, \theta, \phi)| / \sigma(\theta) \right\}} \right), \quad (53)$$

where $\tilde{\mathbf{B}}(\mathbf{W}, \theta, \phi)$ is defined in (6), Π_m is defined in (14), Π_s is defined in (15), and $\sigma(\theta)$ is defined in (21). To evaluate the QoS, the minimum received SNR in SAT service areas is defined as

$$\text{SNR}_{\text{svc}} = \min_{(\theta, \phi) \in \Pi_m} \text{SNR}(\mathbf{W}, \theta, \phi), \quad (54)$$

where $\text{SNR}(\mathbf{W}, \theta, \phi)$ is defined in (24). To evaluate SAT out-of-beam power leakage, the peak received signal power at SAT out-of-beam areas is defined as

$$P_{r, \text{obj}} = \max_{(\theta, \phi) \in \Pi_s} P_r(\mathbf{W}, \theta, \phi), \quad (55)$$

where $P_r(\mathbf{W}, \theta, \phi)$ is defined in (22). Lastly, to demonstrate the CMC achievability, we define

$$\eta_{\text{CMC}} = \frac{\max\{|\mathbf{W}|_{m,n}\}}{\min\{|\mathbf{W}|_{m,n}\}}, \quad \forall m \in \mathbb{Z}_{M_x}, n \in \mathbb{Z}_{M_y}. \quad (56)$$

B. Parameter Settings

Parameter	Symbol	Value	Units
SAT altitude	h	550	km
Earth radius	R_e	6370	km
Carrier frequency	f_c	12	GHz
Channel bandwidth	f_{BW}	500	MHz
Path loss parameter (20)	L_0	171.63	dB
Receive antenna gain	G_R	39.7 [36]	dBi
Noise factor	N_f	1.2 [36]	dB
Antenna temperature	T_a	150 [36]	K
Standard temperature	T_0	290	K
Boltzmann constant	k	-228.6	dBW/K/Hz
Antenna-gain-to-noise-temperature	G/T	16 [36]	dB/K

TABLE I: LEO SAT system parameters for Ku-band user downlink.

LEO SAT system parameters for Ku-band user downlink is shown in Table I. We select URA size as $M_x \times M_y = 32 \times 32$, subarray size as $Q_x \times Q_y = 8 \times 8$, and the total number of RF chains and PAs is $N_x \times N_y = 4 \times 4$. Suppose the same PA is utilized across the array. We set PA gain factor $\beta = 1000$, i.e., 30 [dB], PA maximum output power be 2 [W], and PA backoff value be 5 [dB] [36]. Then PA average power can be calculated as $P_{\text{PA,avg}} = 2 \cdot 10^{-5/10} = 0.63$ [W], and the transmit signal power can be obtained by (12) as $P_T = P_{\text{PA,avg}} \cdot (N_x \times N_y) = 10.08$ [W]. According to (10) and the CMC (i.e., $|\mathbf{W}|_{m,l} = 1$), the source signal power is set as $P_s = \frac{P_{\text{PA,avg}}}{\beta Q_x Q_y} = 9.84 \cdot 10^{-6}$ [W]. Also, losses in (19) are set as $L_{c,T} = L_{c,R} = 1$ [dB], $L_a = 0.5$ [dB], $L_{\text{sm}} = 0$ [dB] and $L_{\text{sl}} = 0.3$ [dB] [36]. Then we obtain $L_0 = 171.63$ [dB] from (20).

SAT service beamwidths Θ_{bw} are specified as 10° , 30° , and 60° . Θ_m and Θ_s are set in Table II with varying choices of θ_{svc} and θ_s^* . Also, the SAT FoV angle $\theta_e \approx 67^\circ$ can be obtained through (13). In all the cases, we let the transmit signal power be the same, and have the total power limitation

Beamwidth Θ_{bw}	10°	30°	60°	
ULA main lobe angle set Θ_m	$[-\theta_{\text{svc}}, \theta_{\text{svc}}]$	$[-5^\circ, 5^\circ]$	$[-15^\circ, 15^\circ]$	$[-30^\circ, 30^\circ]$
ULA sidelobe angle set Θ_s	$[-\theta_e, -\theta_s^*] \cup [\theta_s^*, \theta_e]$	$[-67^\circ, -10^\circ] \cup [10^\circ, 67^\circ]$	$[-67^\circ, -20^\circ] \cup [20^\circ, 67^\circ]$	$[-67^\circ, -35^\circ] \cup [35^\circ, 67^\circ]$
SNR $_{\text{min}}$	(25b)	11 dB	5 dB	-2 dB
α	(28)	179.35 = 22.54 [dB]	89.89 = 19.54 [dB]	40.15 = 16.04 [dB]

TABLE II: ULA main lobe angle set Θ_m , ULA sidelobe angle set Θ_s , SNR $_{\text{min}}$, and α settings.

$P_T = 10.08$ [W]. To provide larger capacity in SAT service areas, SNR $_{\text{min}}$ in the constraint (25b) is eager to be set as large as possible. However, the total power in the spatial domain should meet the total power limitation according to Parseval's theorem [31]. We can infer that a lower main lobe level can be attained as the beamwidth becomes larger, and the problem (49) and (50) would be infeasible if SNR $_{\text{min}}$ is set too large. Given this, SNR $_{\text{min}}$ of different beamwidths are set in Table II. Also, we refer to the bit error rate (BER) performance of standard MODCODs used in DVB-S2 provided in [38], and suggest to apply MODCODs of 8PSK 8/9, QPSK 4/5 and QPSK 1/4 when received SNRs are guaranteed to be larger than 11 [dB], 5 [dB] and -2 [dB] in our cases. According to the above settings, α values listed in Table II are calculated by (28). The remaining input parameters in Algorithm 1 are set as: $N_{\text{svc}} = \frac{2\theta_{\text{svc}}}{0.1} + 1$, $N_s = 2(\frac{\theta_e - \theta_s^*}{0.1} + 1)$, $\rho^{(0)} = 0.1$, $p = 0.1$, $\kappa = 5$, $\varepsilon_{\text{rank}} = 10^{-5}$. Parameter settings in (51) and the initial point selection (\mathbf{x}_{init} and \mathbf{y}_{init}) will be introduced more in Section V-C. CVX toolbox [39] is applied to solve the problems (49) and (50), and simulations are carried out on a personal computer with 3.60 GHz AMD Ryzen 7 3700X, 32 GB.

C. Numerical Results and Performance Evaluation

Simulations are carried out to show the effectiveness of Algorithm 1 to achieve out-of-beam radiation suppression, QoS guarantee, and CMC when SAT service beamwidths are $\Theta_{\text{bw}} = 10^\circ, 30^\circ, \text{ and } 60^\circ$. In our trials, we found that the convergence properties of Algorithm 1 can be influenced by the penalty parameter update strategy and the initial point selection. We at first set a fixed penalty parameter $\rho^{(\psi)} = 0.1 \forall \psi$ without using the penalty parameter update strategy in (51). However, Algorithm 1 does not converge when $\Theta_{\text{bw}} = 10^\circ, 30^\circ, \text{ and } 60^\circ$, and $\Lambda_1^{(\psi)}/\Lambda_0^{(\psi)}$ is stuck at 0.24, 0.13, and 0.06 after 200 iterations, respectively. We suppose the reason for not achieving rank-1 convergence could be the insufficient suppression of unfavorable directions (i.e., $\text{Tr}(\mathbf{X}^{(\psi)}\mathbf{V}^{(\psi-1)})$ in (49a)). By this inference, we found that it is helpful for Algorithm 1 to converge when (51) is applied. If the ratio of the largest eigenvalue to the second largest eigenvalue in the consecutive iteration is smaller than κ , the penalty parameter is increased to suppress the unfavorable directions. Conversely, if the algorithm finds the correct directions for rank-1 convergence, the penalty parameter remains. Through our trials, different $\rho^{(0)}$, p and κ settings in (51) may lead to different convergence results. We set $\rho^{(0)} = 0.1$, $p = 0.1$, and $\kappa = 5$ for obtaining the lowest NPSL $_{\text{ULA}}$ results. Moreover, if we select a zero vector as the initial point of Algorithm 1 (i.e., $\mathbf{x}_{\text{init}} = \mathbf{y}_{\text{init}} = \mathbf{0}$) and apply (51), Algorithm 1 converges when $\Theta_{\text{bw}} = 10^\circ$ (at the 33rd iteration) and 30° (at the 33rd iteration), but does

not converge when $\Theta_{\text{bw}} = 60^\circ$ ($\Lambda_1^{(\psi)}/\Lambda_0^{(\psi)}$ is stuck at 0.07 after 200 iterations). While, we found that if [27] is selected as the initial point, Algorithm 1 converges when $\Theta_{\text{bw}} = 60^\circ$ (at the 67th iteration), and so do $\Theta_{\text{bw}} = 10^\circ$ (at the 33rd iteration) and 30° (at the 48th iteration). We suppose [27] a good initial point, particularly for broadened beam cases, due to its constant modulus property and the low complexity associated with a closed-form solution.

1) *Numerical Results:* In Fig. 8a, 8b and 8c, ULA beam patterns $|\mathbf{B}(\mathbf{x}, \vartheta)|$ and patterns of $\frac{|\mathbf{B}(\mathbf{x}, \vartheta)|}{\sqrt{\tilde{\sigma}(\vartheta)}}$ are plotted in orange and blue line, respectively. The ULA beampatterns $|\mathbf{B}(\mathbf{x}, \vartheta)|$ feature the main lobe lower bound and sidelobe upper bound follow the shape of $\tilde{\sigma}(\vartheta)$, defined in (38), which is highlighted in red curves. While, pattern of $\frac{|\mathbf{B}(\mathbf{x}, \vartheta)|}{\sqrt{\tilde{\sigma}(\vartheta)}}$ have a constant level of main lobe lower bound α and sidelobe upper bound t^* . The NPSL $_{\text{ULA}}$ defined in (52) can then be calculated by $20 \log_{10} \left(\frac{t^*}{\alpha} \right)$ listed in Table III. In each case, the beamforming coefficients meet CMC as shown in Fig. 8d. The URA beampatterns $|\tilde{\mathbf{B}}(\mathbf{W}, \theta, \phi)|$ are generated by the ULA beampatterns by (30). In Fig. 9a, 10a and 11a, the URA beampatterns are depicted in $\sin(\theta) \cos(\phi) - \sin(\theta) \sin(\phi)$ plane. Through our method, the URA beampattern main lobe region is square and PSL of the URA beampattern lies in its cross-region (i.e., when $\phi = 0^\circ/90^\circ$) which verify the inference in Fig. 6b. To evaluate $P_{r, \text{oob}}$ defined in (55), the received signal power $P_r(\mathbf{W}, \theta, \phi)$ at $\phi = 0^\circ$ of each case is plotted in Fig. 9b, 10b and 11b. Low $P_{r, \text{oob}}$ can be achieved to prevent interference with UTs in SAT out-of-beam areas. Moreover, the received SNR of each case is calculated by (24) and depicted in Fig. 9c, 10c and 11c. The received SNR along $\phi = 0^\circ/45^\circ$ are plotted in Fig. 9d, 10d and 11d. We can observe that the SNR lower bound in SAT service areas is larger than or equal to SNR $_{\text{min}}$ set in Table II in all cases. The QoS is guaranteed since we consider the path loss variation from SAT to UT due to the Earth's curvature when synthesizing beampattern inspired by the isoflux radiation patterns in [9]–[13]. In Table III, performance evaluation made by the metrics defined in Section V-A are listed.

Beamwidth Θ_{bw}	10°	30°	60°
NPSL $_{\text{ULA}}$ [dB]	-16.41	-15.43	-16.1
NPSL $_{\text{URA}}$ [dB]	-7.39	-14.59	-16.39
SNR $_{\text{svc}}$ [dB]	11.02	5	-2
$P_{r, \text{oob}}$ [dBm]	-59.26	-66.94	-75.69
η_{CMC}	1	1	1

TABLE III: Performance evaluation of the proposed algorithm with the metrics defined in Section V-A.

2) *Comparison with Other Works:* First, the proposed algorithm is compared with [9]–[11], [13] that consider the synthesis of isoflux radiation pattern but without considering CMC. The numerical results of each paper are listed in Table IV. In [9]–[11], [13], evolutionary algorithms are applied and

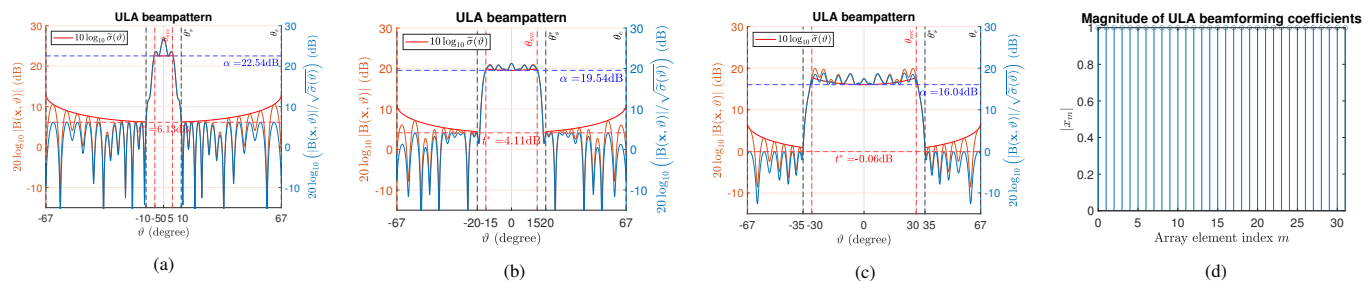


Fig. 8: ULA beampattern $|B(\mathbf{x}, \vartheta)|$ and pattern of $\frac{|B(\mathbf{x}, \vartheta)|}{\sqrt{\sigma(\vartheta)}}$ obtained by Algorithm 1 when beamwidths are (a) $\Theta_{\text{bw}} = 10^\circ$, (b) $\Theta_{\text{bw}} = 30^\circ$ and (c) $\Theta_{\text{bw}} = 60^\circ$. (d) Magnitude of ULA beamforming coefficients $|x_m|$ when $\Theta_{\text{bw}} = 10^\circ, 30^\circ$ and 60° .

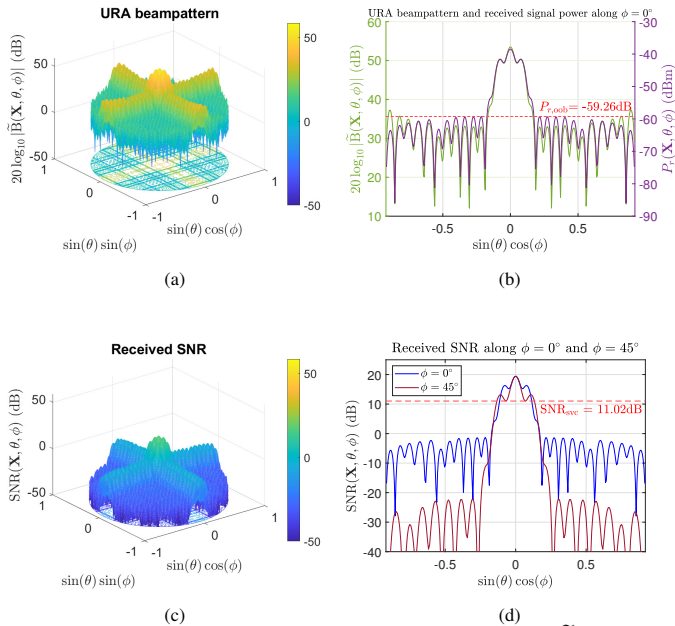


Fig. 9: Results of $\Theta_{\text{bw}} = 10^\circ$ (a) URA beampattern $|\tilde{B}(\mathbf{W}, \theta, \phi)|$, (b) received signal power $P_r(\mathbf{W}, \theta, \phi)$ at $\phi = 0^\circ$, (c) received SNR $\text{SNR}(\mathbf{W}, \theta, \phi)$ and (d) received SNR along $\phi = 0^\circ/45^\circ$.

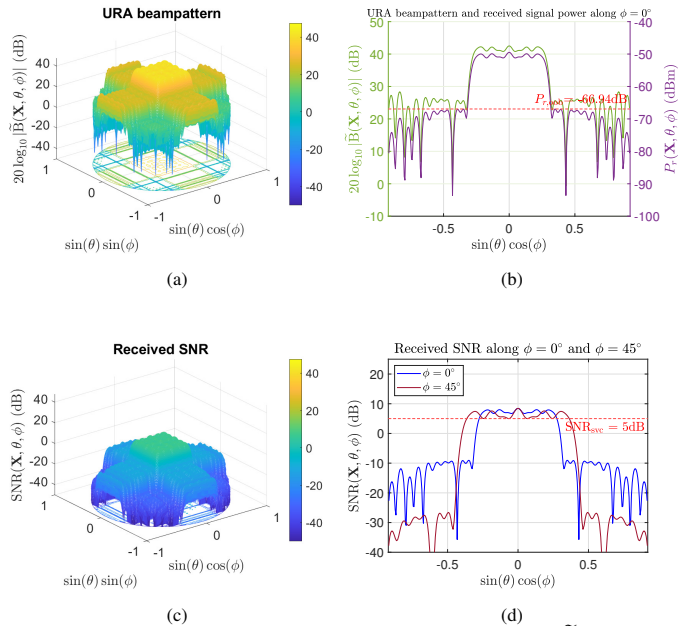


Fig. 10: Results of $\Theta_{\text{bw}} = 30^\circ$ (a) URA beampattern $|\tilde{B}(\mathbf{W}, \theta, \phi)|$, (b) received signal power $P_r(\mathbf{W}, \theta, \phi)$ at $\phi = 0^\circ$, (c) received SNR $\text{SNR}(\mathbf{W}, \theta, \phi)$ and (d) received SNR along $\phi = 0^\circ/45^\circ$.

$\eta_{\text{CMC}} \neq 1$ as they did not consider CMC. In Fig. 12, the results of [13] are compared with the proposed algorithm. A ULA of $M = 10$ is considered. Parameters of the proposed algorithm are set as $(\theta_{\text{svc}}, \theta_s^*, \theta_e) = (8^\circ, 17^\circ, 67^\circ)$, $\text{SNR}_{\text{min}} = 0$ [dB] and other parameters remain the same in Section V-B. In Fig. 12a, the NPSL_{ULA} obtained through [13] and the proposed algorithm are -20.26 [dB] and -10.76 [dB], respectively. From Fig. 12b, the proposed algorithm achieves CMC with $\eta_{\text{CMC}} = 1$. While, [13] did not achieve CMC and its $\eta_{\text{CMC}} = 11.95$. As CMC greatly reduces the degree of freedom, it is foreseeable that lower NPSL_{ULA} can be achieved in [13]. Although [13] can attain lower NPSL_{ULA} , its η_{CMC} is as high as 11.95 which is not favored for maximizing PAs efficiency and may not be practical for LEO SAT application. One possible reason for not considering CMC in [9]–[11], [13] could be the difficulties of considering equality constraints in evolutionary algorithms [18]–[20].

In Fig. 13, the proposed algorithm is compared with the ADMM-based algorithm in [25] which considered broadened beam ULA design with CMC but without the synthesis of isoflux radiation pattern. A ULA of $M = 32$ is

considered. The parameters of the proposed algorithm are set as $(\theta_{\text{svc}}, \theta_s^*, \theta_e) = (30^\circ, 35^\circ, 67^\circ)$, $\text{SNR}_{\text{min}} = -1.3$ [dB] and other parameters remain the same in Section V-B. The main lobe angle set of [25] is set as $[-30^\circ, 30^\circ]$ with mainlobe variation ± 1.17 [dB], sidelobe angle set is $[-90^\circ, -35^\circ] \cup [35^\circ, 90^\circ]$, and penalty parameters are $\rho_1 = 1$ and $\rho_2 = 0.5$. Also, we apply [27] as the initial point of the algorithm in [25] since the algorithm does not converge if a zero vector is chosen as the initial point proposed in [25]. In Fig. 13a, our result features the beampattern main lobe lower bound and sidelobe upper bound shaped by the curve of $\tilde{\sigma}(\vartheta)$. While, [25] has a constant level of sidelobe upper bound and main lobe variation is limited in a given range. We do not consider main lobe upper bound constraint since only the main lobe lower bound should be constrained for QoS guarantee in our application. The NPSL_{ULA} of [25] and the proposed algorithm are -13.68 [dB] and -16.88 [dB], respectively. (Since [25] does not consider $\tilde{\sigma}(\vartheta)$, we set $\tilde{\sigma}(\vartheta) = 1$ when evaluate its NPSL_{ULA} .) Both algorithms can achieve CMC as shown in Fig. 13b, and our algorithm outperforms [25] to obtain a lower NPSL_{ULA} with a margin of 3.2 [dB].

Paper	Array type/# of array elements	Beamwidth Θ_{bw}	η_{CMC}	NPSL [dB]
[Cai2023] [13]	ULA/16	16°	11.95	-20.26
[Yoshimoto2019] [11]	Non-uniformly spaced linear array/12	90°	7.91	No sidelobe
[Ibarra2015] [10]	Sparse concentric rings array/6 + 8	102.66°	66.31	No sidelobe
[Reyna2012] [9]	URA/10 \times 10	18°	549.5	-16.7
[Reyna2012] [9]	Aperiodic planar array/64	18°	7.12	-17
Proposed algorithm	ULA/16	16°	1	-10.76
Proposed algorithm	URA/32 \times 32	$10^\circ/30^\circ/60^\circ$	1/1/1	-7.39/ -14.59/ -16.39

TABLE IV: Comparison of the synthesis of isoflux radiation pattern in [9]–[11], [13].

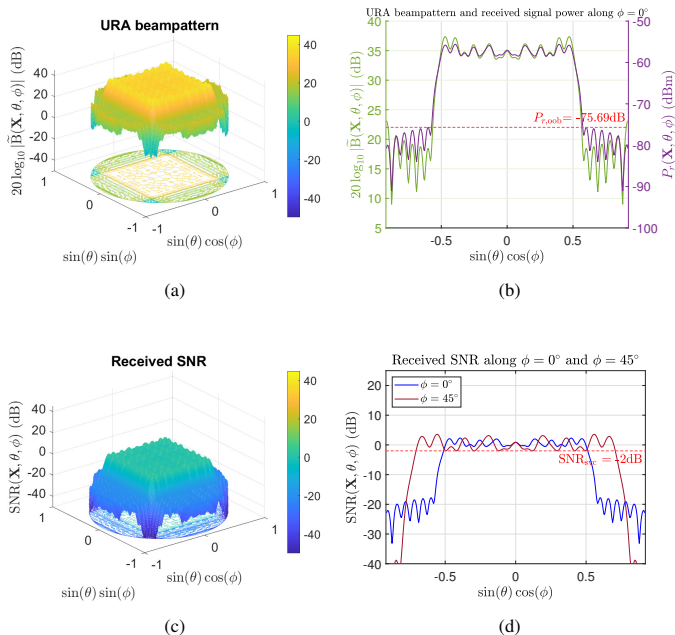
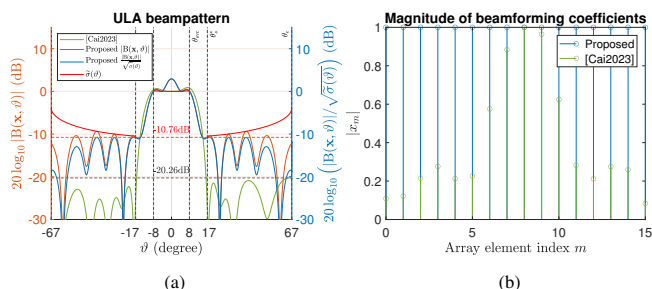
Fig. 11: Results of $\Theta_{\text{bw}} = 60^\circ$ (a) URA beam pattern $|\tilde{\mathbf{B}}(\mathbf{W}, \theta, \phi)|$, (b) received signal power $P_r(\mathbf{W}, \theta, \phi)$ at $\phi = 0^\circ$, (c) received SNR $\text{SNR}(\mathbf{W}, \theta, \phi)$ and (d) received SNR along $\phi = 0^\circ/45^\circ$.

Fig. 12: Comparison of the proposed algorithm with [Cai2023] [13] which considered the synthesis of isoflux radiation pattern but without CMC: (a) ULA beam pattern and (b) magnitude of beamforming coefficients.

D. Channel Capacity Evaluation

To show that the proposed method is applicable for LEO broadcasting applications such as digital video broadcasting (DVB), we compare the capacity of the proposed “broadened-beam” beamformers with that of “narrow-beam” beamformer utilizing an array steering vector [6]–[8]. If beamforming is realized by adjusting the transmitted signal phase according to the array steering vector, the beamformer 3dB beamwidth can be evaluated as [31]

$$\Theta^{\text{3dB}} = \sin^{-1} \left(\frac{0.891\lambda_c}{d_a} \right) \text{ [deg]}, \quad (57)$$

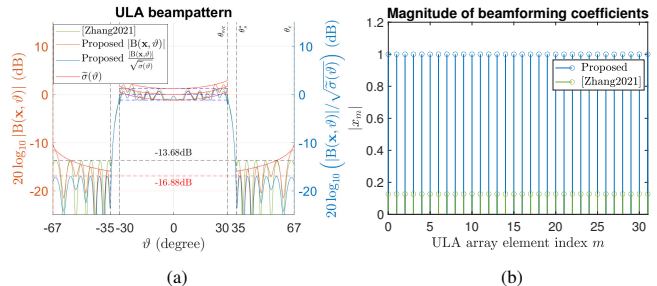


Fig. 13: Comparison of the proposed algorithm with [Zhang2021] [25] which considered CMC but without the synthesis of isoflux radiation pattern: (a) ULA beam pattern and (b) magnitude of beamforming coefficients.

where λ_c is the signal wavelength, $d_a = (M - 1)d_e$ is the array length and d_e is the antenna element spacing. For a URA with size 32×32 (i.e., $M = 32$) and element spacing $d_e = \frac{\lambda_c}{2}$, we have $\Theta^{\text{3dB}} = 3.3^\circ$. Let $\mathbf{W}_{\text{b}, \Theta_{\text{bw}}}$ be the beamforming coefficient matrix of “broadened-beam” beamformer with service beamwidth Θ_{bw} obtained by Algorithm 1. Also, the beamforming coefficient matrix of “narrow-beam” beamformer is denoted as \mathbf{W}_{n} , and we set $[\mathbf{W}_{\text{n}}]_{m,l} = |[\mathbf{W}_{\text{b}, \Theta_{\text{bw}}}]_{m,l}| = 1, \forall m, l \in \mathbb{Z}_M$ (due to CMC) to compare channel capacity with “broadened-beam” beamformer under the same total weight magnitude values. The beam pattern value of “narrow-beam” beamformer at its main lobe direction $(\theta, \phi) = (0, 0)$ is

$$D_{\text{n}, \text{ML}} = |\tilde{\mathbf{B}}(\mathbf{W}_{\text{n}}, 0, 0)|^2 = M^4, \quad (58)$$

where $\tilde{\mathbf{B}}(\mathbf{W}_{\text{n}}, \theta, \phi)$ is defined in (6). Let the main lobe region of “narrow-beam” beamformer be defined within its 3dB beamwidth Θ^{3dB} , we have

$$|\tilde{\mathbf{B}}(\mathbf{W}_{\text{n}}, \theta, \phi)|^2 \geq 0.5 D_{\text{n}, \text{ML}}, \forall \theta \in [0, \frac{\Theta^{\text{3dB}}}{2}], \forall \phi \in [0, 2\pi]. \quad (59)$$

According to (24), the minimum received SNR that “narrow-beam” beamformer can provide within its 3dB beamwidth is defined as

$$\text{SNR}_{\text{n}} = \frac{\beta G_R P_s (0.5 D_{\text{n}, \text{ML}})}{\sigma^2(\theta) L_0 k T_{\text{sys}} f_{\text{BW}}}. \quad (60)$$

Also, $\text{SNR}_{\text{b}, \Theta_{\text{bw}}}$ is denoted as the minimum received SNR that “broadened-beam” beamformer can provide within its service beamwidth Θ_{bw} . The channel capacity of “broadened-beam” and “narrow-beam” beamformers that can provide within their service beamwidths are evaluated based on Shannon’s capacity [40]:

$$C_{\text{b}, \Theta_{\text{bw}}} = f_{\text{BW}} \log_2(1 + \text{SNR}_{\text{b}, \Theta_{\text{bw}}}), \quad (61)$$

$$C_{\text{n}} = f_{\text{BW}} \log_2(1 + \text{SNR}_{\text{n}}). \quad (62)$$

Moreover, the beam service areas of the “broadened-beam” beamformer with beamwidth Θ_{bw} is denoted as $A_{\text{b}, \Theta_{\text{bw}}}$. The

beam service areas of the “narrow-beam” beamformer with 3dB beamwidth under beam steering angle is denoted as $A_{n,\Theta_{\theta_T}^{3dB}}$, where $\Theta_{\theta_T}^{3dB}$ is the 3dB beamwidth under beam steering angle θ_T [31]

$$\Theta_{\theta_T}^{3dB} = \sin^{-1} \left(\sin(\theta_T) + \frac{0.443\lambda_c}{d_a} \right) - \sin^{-1} \left(\sin(\theta_T) - \frac{0.443\lambda_c}{d_a} \right), \quad (63)$$

where $d_a = (M - 1)d_e$. Note that when $\theta_T = 0$, $\Theta_{\theta_T}^{3dB}$ can be approximated by Θ^{3dB} (defined in (57)) through small angle approximation [31]. Values of $A_{b,\Theta_{bw}}$ when $\Theta_{bw} = 10^\circ$, 30° and 60° are shown in Table V which is calculated by (17). Also, values of $A_{n,\Theta_{\theta_T}^{3dB}}$ when beam steering angle is $\theta_T = 0^\circ$ (no steering), $\frac{10^\circ}{2}$, $\frac{30^\circ}{2}$, and $\frac{60^\circ}{2}$ are shown in Table VI which is estimated according to Appendix A. Assume UTs are uniformly distributed within $A_{b,\Theta_{bw}}$. Compared with the “broadened-beam” beamformer that can serve UTs within $A_{b,\Theta_{bw}}$ per single beam, it takes “narrow-beam” beamformer several time slots for steering and serving all UTs within $A_{b,\Theta_{bw}}$. The beam transition time increases in proportion to $N_{n,\Theta_{bw}}^{(min)}$ denoted as the minimum number of beams that the “narrow-beam” beamformer is needed to cover the beam service areas of “broadened-beam” beamformer $A_{b,\Theta_{bw}}$. $N_{n,\Theta_{bw}}^{(min)}$ with $\Theta_{bw} = 10^\circ$, 30° , and 60° are evaluated as follows

$$N_{n,10}^{(min)} = \left\lceil \frac{A_{b,10}}{A_{n,\Theta_5^{3dB}}} \right\rceil, N_{n,30}^{(min)} = N_{n,10}^{(min)} + \left\lceil \frac{A_{b,30} - A_{b,10}}{A_{n,\Theta_{15}^{3dB}}} \right\rceil, \quad (64)$$

$$N_{n,60}^{(min)} = N_{n,30}^{(min)} + \left\lceil \frac{A_{b,60} - A_{b,30}}{A_{n,\Theta_{30}^{3dB}}} \right\rceil.$$

Taking beam transition time into consideration, the average channel capacity of the “narrow-beam” beamformer for serving UTs in $A_{b,\Theta_{bw}}$ is evaluated as

$$C_{n,\Theta_{bw}} = \frac{C_n}{N_{n,\Theta_{bw}}^{(min)}}, \quad (65)$$

where C_n is evaluated in (62). The values of $C_{b,\Theta_{bw}}$ and $C_{n,\Theta_{bw}}$ are shown in Table VII. From our analysis, the proposed “broadened-beam” beamformers with $\Theta_{bw} = 10^\circ$, 30° , and 60° can offer capacities that are at least four times greater than “narrow-beam” beamformers employing an array steering vector when beam transition time is considered.

Beamwidth Θ_{bw}	10°	30°	60°
$A_{b,\Theta_{bw}}$ [Mkm ²]	7, 279	68, 666	326, 450

TABLE V: Beam areas of “broadened-beam” beamformer $A_{b,\Theta_{bw}}$ under different beamwidths Θ_{bw} .

$\theta_T = \Theta_{bw}/2$	0° (no steering)	$10^\circ/2$	$30^\circ/2$	$60^\circ/2$
$\Theta_{\theta_T}^{3dB}$ [deg]	3.3°	3.35°	3.41°	3.81°
$A_{n,\Theta_{\theta_T}^{3dB}}$ [Mkm ²]	786.23	820.12	1, 203.9	5, 741.8

TABLE VI: Beam areas of “narrow-beam” beamformer $A_{n,\Theta_{\theta_T}^{3dB}}$ with 3dB beamwidth $\Theta_{\theta_T}^{3dB}$ under different steering angles θ_T .

VI. CONCLUSION

In this paper, beam-broadening algorithms for uniform rectangular array (URA) in low Earth orbit (LEO) satellite communications (SatComs) were studied. The proposed method is the first of its kind that jointly considers the path loss variation from satellite (SAT) to user terminal (UT) due to the Earth’s curvature to guarantee quality of service (QoS),

Beamwidth Θ_{bw}	10°	30°	60°	Remark
$D_{n,ML}$	1, 048, 576			(58)
SNR _n [dB]	23.12			(60)
C_n [Mbps]	3, 844			(62)
SNR _{b,\Theta_{bw}}} [dB]	11.02	5	-2	Table II
$\alpha_{\Theta_{bw}}$	179.35	89.89	40.15	Table II
$N_{n,\Theta_{bw}}^{(min)}$	9	60	105	(64)
$C_{n,\Theta_{bw}}$ [Mbps]	427.11	64.07	36.61	(65)
$C_{b,\Theta_{bw}}$ [Mbps]	1, 882.2	1, 028.7	352.86	(61)

TABLE VII: Channel capacity evaluation of “broadened-beam” beamformer and “narrow-beam” beamformer employing an array steering vector.

constant modulus constraint (CMC) for maximizing power amplifier (PA) efficiency, and out-of-beam radiation suppression to avoid interference. The URA design problem is formulated and decomposed into two uniform linear array (ULA) design subproblems with the idea of Kronecker product beamforming to alleviate the computational complexity. The non-convex ULA subproblems are solved by a convex iterative algorithm. Simulation results demonstrate the proposed method that can synthesize beampattern with low out-of-beam radiation, achieve CMC, and guarantee the received SNR in SAT service areas when service beamwidths are 10° , 30° , and 60° . Besides, the channel capacity evaluation shows that the proposed “broadened-beam” beamformers can offer capacities that are at least four times greater than “narrow-beam” beamformers employing an array steering vector when beam transition time is taken into account. Therefore, the proposed method is a potential candidate for LEO broadcasting applications such as digital video broadcasting (DVB). In the future, an algorithm that can directly solve the URA design problem (25) with a large antenna size, e.g., 32×32 , is worthwhile developing to achieve optimal out-of-beam radiation suppression once the computational complexity issues are overcome.

APPENDIX A BEAM AREAS ESTIMATION OF “NARROW-BEAM” BEAMFORMER WITH BEAM STEERING ANGLE θ_T

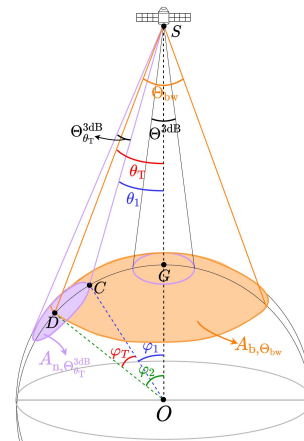


Fig. 14: Diagram for estimating $A_{n,\Theta_{\theta_T}^{3dB}}$.

In Fig. 14, $A_{n,\Theta_{\theta_T}^{3dB}}$ is the beam service areas of the “narrow-beam” beamformer with beam steering angle θ_T that we would like to estimate. $\Theta_{\theta_T}^{3dB}$ and Θ^{3dB} are the “narrow-beam” beamformer 3dB beamwidth with and without beam steering

defined in (63) and (57), respectively. Also, $A_{b, \Theta_{bw}}$ is the beam service areas of the “broadened-beam” beamformer with service beamwidth Θ_{bw} . $A_{n, \Theta_{\theta_T}^{3dB}}$ can be estimated according to the following steps: Firstly, calculate $\Theta_{\theta_T}^{3dB}$ according to (63). Then, we have $\theta_1 = \theta_T - \Theta_{\theta_T}^{3dB}/2$. Secondly, from ΔOCS , φ_1 can be obtained by (18). Similarly, from ΔODS , φ_2 can be obtained by (18). Then, we have $\varphi_T = \varphi_2 - \varphi_1$. Lastly, $A_{n, \Theta_{\theta_T}^{3dB}}$ is obtained by (17).

REFERENCES

- [1] O. Kodheli, E. Lagunas, N. Maturo, S. K. Sharma, B. Shankar, J. F. M. Montoya, J. C. M. Duncan, D. Spano, S. Chatzinotas, S. Kisseleff, J. Querol, L. Lei, T. X. Vu, and G. Goussetis, “Satellite Communications in the New Space Era: A Survey and Future Challenges,” *IEEE Communications Surveys & Tutorials*, vol. 23, no. 1, pp. 70–109, 2021.
- [2] Y. Lu and X. Zheng, “6G: A survey on technologies, scenarios, challenges, and the related issues,” *Journal of Industrial Information Integration*, vol. 19, p. 100158, 2020.
- [3] 3GPP TS 23.501, “Technical Specification Group Services and System Aspects; System architecture for the 5G System (5GS); Stage 2; (Release 18);” December 2023.
- [4] O. B. Osoro and E. J. Oughton, “A Techno-Economic Framework for Satellite Networks Applied to Low Earth Orbit Constellations: Assessing Starlink, OneWeb and Kuiper,” *IEEE Access*, vol. 9, pp. 141 611–141 625, 2021.
- [5] M. A. Richards, *Fundamentals of Radar Signal Processing*. McGraw-Hill Professional, June 2005.
- [6] J. Tang, D. Bian, G. Li, J. Hu, and J. Cheng, “Optimization Method of Dynamic Beam Position for LEO Beam-Hopping Satellite Communication Systems,” *IEEE Access*, vol. 9, pp. 57 578–57 588, 2021.
- [7] X. Hu, Y. Zhang, X. Liao, Z. Liu, W. Wang, and F. M. Ghannouchi, “Dynamic Beam Hopping Method Based on Multi-Objective Deep Reinforcement Learning for Next Generation Satellite Broadband Systems,” *IEEE Transactions on Broadcasting*, vol. 66, no. 3, pp. 630–646, 2020.
- [8] L. Lei, E. Lagunas, Y. Yuan, M. G. Kibria, S. Chatzinotas, and B. Ottersten, “Beam Illumination Pattern Design in Satellite Networks: Learning and Optimization for Efficient Beam Hopping,” *IEEE Access*, vol. 8, pp. 136 655–136 667, 2020.
- [9] A. Reyna, M. A. Panduro, and C. del Rio-Bocio, “Design of aperiodic planar arrays for isoflux radiation in geo satellites by applying evolutionary optimization,” *Expert Systems with Applications*, vol. 39, no. 8, pp. 6872–6878, 2012.
- [10] M. Ibarra, M. A. Panduro, Ángel G. Andrade, and A. Reyna, “Design of sparse concentric rings array for LEO satellites,” *Journal of Electromagnetic Waves and Applications*, vol. 29, no. 15, pp. 1983–2001, 2015.
- [11] E. Yoshimoto and M. V. T. Heckler, “Optimization of Planar Antenna Arrays Using the Firefly Algorithm,” *Journal of Microwaves, Optoelectronics and Electromagnetic Applications*, vol. 18, no. 1, p. 126–140, Jan 2019.
- [12] F. Zeng, Z.-Y. Zhang, Y. Feng, S. Zuo, C. Zhang, and L. Wang, “Wideband circularly polarised antenna array with isoflux pattern,” *IET Microwaves, Antennas & Propagation*, vol. 15, no. 9, pp. 1025–1034, 2021.
- [13] M. Cai, W. Li, X. Shi, Q. Zhang, H. Liu, and Y. Li, “An Innovative Design of Isoflux Scanning Digital Phased Array Based on Completely Shared Subarray Architecture for Geostationary Satellites,” *Electronics*, vol. 12, no. 18, 2023.
- [14] Y. Li, Y. Huang, M. H. Nielsen, F. Jalili, W. Wei, J. Ren, Y. Yin, M. Shen, and G. F. Pedersen, “A Cross-Mode Universal Digital Pre-Distortion Technology for Low-Sidelobe Active Antenna Arrays in 5G and Satellite Communications,” *Electronics*, vol. 10, no. 16, 2021.
- [15] E. G. Larsson and L. Van Der Perre, “Out-of-Band Radiation From Antenna Arrays Clarified,” *IEEE Wireless Communications Letters*, vol. 7, no. 4, pp. 610–613, 2018.
- [16] N. Tervo, B. Khan, J. P. Aikio, O. Kursu, M. Jokinen, M. E. Leinonen, M. Sonkki, T. Rahkonen, and A. Pärssinen, “Combined Sidelobe Reduction and Omnidirectional Linearization of Phased Array by Using Tapered Power Amplifier Biasing and Digital Predistortion,” *IEEE Transactions on Microwave Theory and Techniques*, vol. 69, no. 9, pp. 4284–4299, 2021.
- [17] A. Piacibello, R. Giofrè, R. Quaglia, R. Figueiredo, N. Carvalho, P. Colantonio, V. Valenta, and V. Camarchia, “A 5-W GaN Doherty Amplifier for Ka-Band Satellite Downlink With 4-GHz Bandwidth and 17-dB NPR,” *IEEE Microwave and Wireless Components Letters*, vol. 32, no. 8, pp. 964–967, 2022.
- [18] A. S. Barkat Ullah, R. Sarker, and C. Lokan, “Handling equality constraints in evolutionary optimization,” *European Journal of Operational Research*, vol. 221, no. 3, pp. 480–490, 2012.
- [19] M. Ming, A. Trivedi, R. Wang, D. Srinivasan, and T. Zhang, “A Dual-Population-Based Evolutionary Algorithm for Constrained Multiobjective Optimization,” *IEEE Transactions on Evolutionary Computation*, vol. 25, no. 4, pp. 739–753, 2021.
- [20] Y. Tian, T. Zhang, J. Xiao, X. Zhang, and Y. Jin, “A Coevolutionary Framework for Constrained Multiobjective Optimization Problems,” *IEEE Transactions on Evolutionary Computation*, vol. 25, no. 1, pp. 102–116, 2021.
- [21] B. Fuchs, “Application of Convex Relaxation to Array Synthesis Problems,” *IEEE Transactions on Antennas and Propagation*, vol. 62, no. 2, pp. 634–640, 2014.
- [22] Y. Liu, J. Bai, K. D. Xu, Z. Xu, F. Han, Q. H. Liu, and Y. Jay Guo, “Linearly Polarized Shaped Power Pattern Synthesis With Sidelobe and Cross-Polarization Control by Using Semidefinite Relaxation,” *IEEE Transactions on Antennas and Propagation*, vol. 66, no. 6, pp. 3207–3212, 2018.
- [23] Z. Xu, Y. Liu, M. Li, and Y. Li, “Linearly Polarized Shaped Power Pattern Synthesis With Dynamic Range Ratio Control for Arbitrary Antenna Arrays,” *IEEE Access*, vol. 7, pp. 53 621–53 628, 2019.
- [24] J. Liang, X. Fan, H. C. So, and D. Zhou, “Array Beampattern Synthesis Without Specifying Lobe Level Masks,” *IEEE Transactions on Antennas and Propagation*, vol. 68, no. 6, pp. 4526–4539, 2020.
- [25] X. Zhang, X. Wang, and H. C. So, “Linear Arbitrary Array Pattern Synthesis With Shape Constraints and Excitation Range Control,” *IEEE Antennas and Wireless Propagation Letters*, vol. 20, no. 6, pp. 1018–1022, 2021.
- [26] S. Lei, W. Yang, Z. Lin, Z. He, H. Hu, Z. Zhao, and Y. Bao, “An Excitation-DRR Control Approach for Wide-Beam Power Gain Pattern Synthesis,” *Signal Processing*, vol. 204, p. 108858, 2023.
- [27] C. Fonteneau, M. Crussière, and B. Jahan, “A Systematic Beam Broadening Method for Large Phased Arrays,” in *2021 Joint European Conference on Networks and Communications & 6G Summit (EuCNC/6G Summit)*, 2021, pp. 7–12.
- [28] A. Frank and I. Cohen, “Constant-Beamwidth Kronecker Product Beamforming With Nonuniform Planar Arrays,” *Frontiers in Signal Processing*, vol. 2, 2022.
- [29] I. Cohen, J. Benesty, and J. Chen, “Differential Kronecker Product Beamforming,” *IEEE/ACM Transactions on Audio, Speech, and Language Processing*, vol. 27, no. 5, pp. 892–902, 2019.
- [30] Y. Albagory and F. Alraddady, “Optimum Extrapolation Techniques for Two-Dimensional Antenna Array Tapered Beamforming,” *Electronics*, vol. 11, no. 13, 2022.
- [31] H. Trees, *Optimum Array Processing – Part IV of Detection, Estimation, and Modulation Theory*, May 2002.
- [32] J. G. Proakis and M. Salehi, *Fundamentals of communication systems / John G. Proakis, Masoud Salehi*. Upper Saddle River, N.J: Pearson Prentice Hall, 2005.
- [33] A. Tapatugssanagorn, K. Umebayashi, J. Lehtomäki, and C. Pomalaza-Ráez, “Analysis of the effect of nonlinear low noise amplifier with memory for wideband spectrum sensing,” in *1st International Conference on 5G for Ubiquitous Connectivity*, 2014, pp. 87–91.
- [34] H. A. Dell, “Introduction to Radar Systems. Merrill I. Skolnik. McGraw-Hill Book Co., London and New York. 1962. 648 pp. Illustrated. £5 12s. 6d.” *The Journal of the Royal Aeronautical Society*, vol. 67, pp. 313 – 313, 1963.
- [35] A. Polyani and A. Manzhurov, *Handbook of Mathematics for Engineers and Scientists*, 11 2006.
- [36] G. T. 38.821, “Solutions for NR to support non-terrestrial networks (NTN); (release 16);” March 2023.
- [37] J. Dattorro, *Convex Optimization & Euclidean Distance Geometry*. Meboo Publishing USA, 2005.
- [38] A.-u. Rahman, S. Dash, and A. K. Luhach, “Dynamic MODCOD and power allocation in DVB-S2: a hybrid intelligent approach,” *Telecommunication Systems*, vol. 76, pp. 49–61, 2021.
- [39] M. Grant and S. Boyd, “CVX: Matlab Software for Disciplined Convex Programming, version 2.1,” <http://cvxr.com/cvx>, Mar. 2014.
- [40] C. E. Shannon, “A Mathematical Theory of Communication,” *The Bell System Technical Journal*, vol. 27, pp. 379–423, 1948.